CAL LAB

THE INTERNATIONAL JOURNAL OF METROLOGY

METROLOGY 101: CALIBRATING 1 MW 50 MHZ POWER REFERENCE OUTPUT

Comparison of Uncertainty Calculation Models

Calibrating Low-Temperature Radiation Thermometers

Alaska Metrology & Calibration Services

2012
JANUARY
FEBRUARY
MARCH

You have a big job.

Now there's a complete calibration software system to match.

New Fluke Calibration MET/CAL® *Plus* 8.0 software: the only all-in-one calibration software solution that measures up to the task.

Your job is tough. You need to increase productivity and throughput with a more complex, higher-volume workload. And you need to reduce costs while maintaining high accuracy, traceability, and extensive documentation. New Fluke Calibration MET/CAL *Plus* Calibration Management Software version 8.0 includes everything you need to address those needs.

Its comprehensive calibration automation, tracking, documentation, and reporting capabilities can increase productivity by up to 80 %.

See for yourself. Download free MET/CAL *Plus* 8.0 demo software and get more product information at www.flukecal.com/metcal8

FLUKE® Calibration

Fluke Calibration. *Precision, performance, confidence.*™

Electrical	RF	Temperature	Pressure	Flow	Software

CAL LAB
THE INTERNATIONAL JOURNAL OF METROLOGY

Volume 19, Number 1

www.callabmag.com

FEATURES

DEPARTMENTS

ON THE COVER: Hock Eng Lim sets up the Agilent N432A thermistor power meter to calibrate the 1 mW reference source of an E4419B EPM power meter at an on-site calibration lab in Penang, Malaysia.

CONFERENCES & MEETINGS 2012

Mar 6-8 2012 South East Asia Flow Measurement Conference. Kuala Lumpur, Malaysia. www.tuvnel.com

Mar 8-9 METROMEET – 8th International Conference on Industrial Dimensional Metrology. Bilbao, Spain. http://www.metromeet.org/.

Mar 14-15 Quality Expo Texas. Fort Worth, TX. In 2012, the regional, biennial edition of Quality Expo will move on from Charlotte to join Canon's newest advanced design and manufacturing event planned to launch in Texas. Website: http://www.canontradeshows.com/expo/qexpos10/.

Mar 19-23 Measurement Science Conference. Anaheim, CA. Measurement Science: Challenges in the Future. Held in conjunction with the International Temperature Symposium (ITS9). Website: http://www.msc-conf.com/.

Mar 19-23 9th International Temperature Symposium. Anaheim, CA. The NIST Temperature and Humidity Group has organized the 9th International Temperature Symposium, in conjunction with the Measurement Science Conference. Website: http://www.its9.org/.

Mar 21-23 ICSM2012. Annecy, France. The 3rd International Conference on Surface Metrology. Website: http://www.icsm3.org.

Apr 23-27 CAFMET 2012. Marrakech, Morocco. The African Committee on Metrology (CAFMET) is organizing the 4th International Metrology Conference. Website: http://www.ac-metrology.com/CAFMET2012.

Apr 25-27 The Americas Flow Measurement Conference. Houston, TX. Email events@tuvnel.com for further details. http://www.tuvnel.com.

Apr 26-29 APMAS 2012. Antalya, Turkey. APMAS 2012 intends to be a global forum for researchers and engineers to present and discuss recent innovations and new techniques in Applied Physics and Material Science. Website: http://www.apmas2012.org/.

Apr 30-May 3 ESTECH 2012. Orlando, FL. ESTECH offers attendees a valuable educational experience with conference sessions and continuing education courses in the fields of design, test, and evaluation/product reliability; contamination control; aerospace; and nanotechnology. Interact with leaders from these industries, academia, and government at the 58th Annual Technical Meeting and Exposition of IEST. http://www.iest.org.

May 8-10 LabIndonesia 2012. Jakarta. Indonesia's 2nd Laboratory Analytical Equipment, Instrumentation and Services Exhibition and Conference. For more information, visit: http://www.lab-asia.com/.

May 9-11 Milestones in Metrology IV. Venice, Italy. The conference trailer on the NMi website gives an initial overview of the new structure, atmosphere and topics of

CAL LAB
THE INTERNATIONAL JOURNAL OF METROLOGY

PUBLISHER
MICHAEL L. SCHWARTZ

EDITOR
SITA P. SCHWARTZ

CAL LAB
PO Box 111113
Aurora, CO 80042
TEL 303-317-6670 • FAX 303-317-5295
office@callabmag.com
www.callabmag.com

Subscription fees for 1 year (4 issues)
$50 for USA, $55 Mexico/Canada,
$65 all other countries.
Visit www.callabmag.com to subscribe
or call 303-317-6670
Printed in the USA.

EDITOR'S DESK

Waiting on Spring

Now that I'm of a certain age, my bones and muscles register the cold a bit different… and not in degrees. I descended cold stairs at sunrise this morning to bang on the boiler's gas regulator with a hammer, as is necessary when temperatures dip near zero degrees Fahrenheit. I get to stay inside though, unlike the folks at Alaska Metrology & Calibration Services--they know cold with the pictures to prove it. Their story begins on page 37, highlighting the use of their mobile lab in a part of the world with limited accessibility.

Peter Saunders with the Measurement Standards Laboratory of New Zealand contributed a timely article for us on the calibration of low-temperature radiation thermometers, addressing common errors in the calibration process of this paticular "low-temperature" instrument.

Hening Huang with Teledyne and MSC have allowed us to use his paper, "Comparison of Uncertainty Calculation Models," from last year's Measurement Science Conference in Pasadena, California. In it, he compares three models: the Student's *t* model, Craig model, and Bayesian model.

This issue's Metrology 101 article, "Calibrating 1 mW 50 MHz Power Reference Output," was contributed by Hock Eng Lim (on the cover) with Agilent Technologies. He shows us how to use new standards to calibrate the reference calibration output of a power meter.

Spring officially begins during the 9th International Temperature Symposium and Measurement Science Conference 2012 in Anaheim, California. Bougainvillaeas bloom in mass and bright yellow lemons sit amid deep green foliage in lovely California (sigh), while I'm shoveling and pushing mounds of snow around the yard in Colorado. Personally, I'm anxiously waiting for spring *rain* that tells us winter has released us from its grip, and the hammer sitting on the boiler downstairs can be put away.

Regards,

Sita

1-6 July 2012

Gaylord National Resort,
Washington DC

WASHINGTON DC

CPEM 2012

Conference on Precision Electromagnetic Measurements

The 2012 Conference on Precision Electromagnetic Measurements is hosted by the National Institute of Standards and Technology in Gaithersburg, Maryland, USA, in cooperation with NCSL International and Centro Nacional de Metrologia. The venue for this conference is the Gaylord National Resort, which is a beautiful new hotel located on the Potomac River just minutes outside of Washington D.C. We look forward to seeing you in 2012!

Conference Chair: **Dean Jarrett** dean.jarrett@nist.gov
Technical Program Chair: **James Randa** james.randa@nist.gov

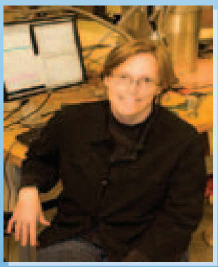

Keynote Speaker
Professor Suzanne Staggs
Princeton University Physics Department

Welcome Remarks: The Metre Convention

Keynote Address: Precision Cosmology

Plenary Talks: Fundamental Constants – the Ultimate Metric; High Harmonic Interferometry; Superconducting Quantum Standards

Special Sessions: Redefinition of the SI; Optical Clocks and the Possible Redefinition of the Second; Graphene Based Electrical Metrology

Emerging Topic Sessions: Terahertz Metrology and Microwave and Antenna Measurements above 100 GHz; Metrology for Smart Grid Applications

Want to see your logo here? Visit http://icpem.org/2012
Limited exhibit space still available.

In accordance with IUPAP principles, CPEM 2012 assures its participants that no scientist will be excluded on the grounds of national origin, nationality, or political considerations unrelated to science.

the conference for the markets of Energy, Oil & Gas, Weighing and Traffic. The complete programme will focus on legal metrology, but this scope will be expanded with the introduction of industrial metrology. During breaks and evening events the focus will shift towards networking and meeting one another. http://www.milestonesinmetrology.com/.

May 13-16 2012 IEEE International Instrumentation and Measurement Technology Conference. Graz, Austria. "Smart Measurements for a Sustainable Environment." http://imtc.ieee-ims.org/.

May 23-25 MetrolExpo2012. Moscow, Russia. The 8th Moscow International Forum "Precise Measurements - The Basis of Quality and Safety" will be held with specialized exhibition of measuring instruments and metrological equipment (MetrolExpo), to ensure uninterrupted operation of production facilities (PromSafety), commercial energy accounting (ResMetering), means of verification and testing of medical devices (MedTest), and the 4th Moscow International Symposium " Accuracy. Quality. Security. " For more information in English visit: http://www.metrol.expoprom.ru/en/.

Jun 20-22 International Symposium on Fluid Flow Measurement. Colorado Springs, CO. http://www.isffm.org/.

Jul 16-20 Coordinate Metrology Systems Conference (CMSC). New Orleans, LA. http://www.cmsc.org/.

SEMINARS: Online & Independent Study

AC-DC Metrology– Self-Paced Online Training. Fluke Training. http://us.flukecal.com/training/courses.

Basic Measuring Tools – Self Directed Learning. The QC Group, http://www.qcgroup.com/calendar/.

Introduction to Measurement and Calibration – Online Training. The QC Group, http://www.qcgroup.com/calendar/.

Intro to Measurement and Calibration – Self-Paced Online Training. Fluke Training. http://us.flukecal.com/training/courses.

ISO/IEC 17025 Compliance. Workplace Training, tel (612) 308-2202, info@wptraining.com, http://www.wptraining.com/.

Measurement Uncertainty – Self-Paced Online Training. Fluke Training. http://us.flukecal.com/training/courses.

Measurement Uncertainty Analysis – Online Training. The QC Group, http://www.qcgroup.com/calendar/.

Metrology for Cal Lab Personnel– Self-Paced Online Training. Fluke Training. http://us.flukecal.com/training/courses.

Precision Dimensional Measurement – Online Training. The QC Group, http://www.qcgroup.com/calendar/.

Precision Measurement Series Level 1. Workplace Training, tel (612) 308-2202, info@wptraining.com, http://www.wptraining.com/.

Precision Electrical Measurement – Self-Paced Online Training. Fluke Training. http://us.flukecal.com/training/courses.

Precision Measurement Series Level 1. Workplace Training, tel (612) 308-2202, info@wptraining.com, http://www.wptraining.com/.

Precision Measurement Series Level 2. Workplace Training, tel (612) 308-2202, info@wptraining.com, http://www.wptraining.com/.

SEMINARS: Dimensional

Feb 21-22 Dimensional Metrology. Los Angeles, CA. Mitutoyo , http://mitutoyo.com, mim@mitutoyo.com.

Feb 23-24 Gage Calibration Systems and Methods. Los Angeles, CA. Mitutoyo , http://mitutoyo.com, mim@mitutoyo.com.

Feb 28-29 Gage Calibration and Repair Workshop. Schaumburg, IL.IICT Training, http://www.iicttraining.com/Schedule.html.

Mar 1-2 Gage Calibration and Repair Workshop. Milwaukee, WI. IICT Training, http://www.iicttraining.com/Schedule.html.

Mar 13-14 Gage Calibration and Repair Workshop. Louisville, KY. IICT Training, http://www.iicttraining.com/Schedule.html.

Mar 13-14 Dimensional Metrology. Boston, MA. Mitutoyo , http://mitutoyo.com, mim@mitutoyo.com.

Mar 15-16 Gage Calibration Systems and Methods. Boston, MA. Mitutoyo , http://mitutoyo.com, mim@mitutoyo.com.

Mar 29-30 Gage Calibration and Repair Workshop. Phoenix, AZ. IICT Training, http://www.iicttraining.com/Schedule.html.

Apr 10-11 Gage Calibration and Repair Workshop. Blaine, MN. IICT Training, http://www.iicttraining.com/Schedule.html.

Apr 16-17 Gage Calibration and Repair Workshop. Atlanta, GA. IICT Training, http://www.iicttraining.com/Schedule.html.

Apr 17-18 Dimensional Metrology. Chicago, IL. Mitutoyo , http://mitutoyo.com, mim@mitutoyo.com.

Apr 19-20 Gage Calibration and Repair Workshop. Myrtle Beach. IICT Training, http://www.iicttraining.com/Schedule.html.

Apr 19-20 Gage Calibration Systems and Methods. Chicago, IL. Mitutoyo , http://mitutoyo.com, mim@mitutoyo.com.

May 14-17 Dimensional and Thermodynamic Calibration Procedures. Las Vegas, NV. Technology Training Inc., http://www.ttiedu.com/schedule.html.

May 15-16 Dimensional Metrology. Cincinnati, OH. Mitutoyo , http://mitutoyo.com, mim@mitutoyo.com.

May 17-18 Gage Calibration Systems and Methods. Cincinnati, OH. Mitutoyo , http://mitutoyo.com, mim@mitutoyo.com.

LEM Voltage & Current Measurement

Voltage Transducers

Provide an Analog Output Signal Magnetically Isolated from the Primary Voltage Circuit

- Full-scale Primary Voltages from ±500V to ±8,000V
- Amplitude Accuracy to ±0.2% at dc
- Amplitude Frequency Response dc to 500kHz (-3dB)

Convert High Voltage Levels in Power Converters to Low Level, Low Impedance Signals that can be Used for Accurate and Safe Test Measurements

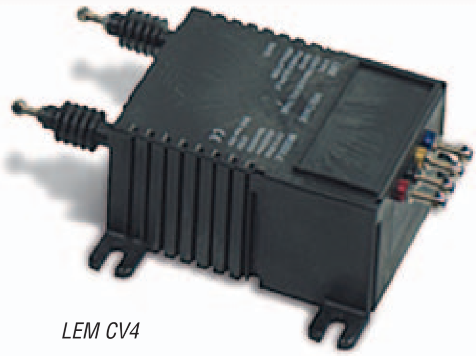

LEM CV4

Closed-Loop Hall Current Transducers

Provide an Analog Output Signal Isolated from the Primary Current Circuit

- Full-scale Primary Currents from ±100A to ±15,000A
- Amplitude Accuracy to ±0.3% at dc
- Amplitude Frequency Response dc to 300kHz (-3dB)
- Common Mode Primary Voltage Isolation
- Split Core Versions Available (±2% at dc)

Suitable for Production Line Testing where Long-term Stability and Reliability are Critical

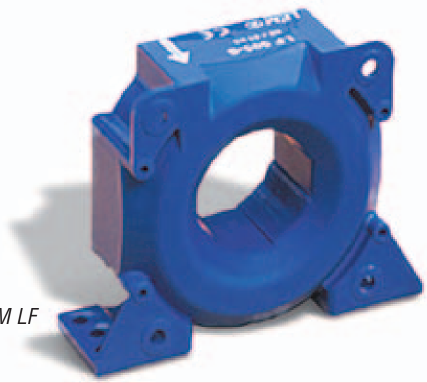

LEM LF

Closed-Loop Fluxgate Current Transducers

Generate a Very High-Accuracy Output Signal with Electrical Isolation from the Primary Circuit

- Full-scale Primary Currents from ±60A to ±1,000A
- Amplitude Linearity to ±0.3ppm at dc
- Amplitude Frequency Response dc to 300kHz (-3dB)
- Very Low Noise to <5ppm rms (dc to 50kHz) gives Wide Dynamic Range
- Very Low Sensitivity to External Current Conductors

For High-accuracy Power Measurements over an Extended Frequency Range

LEM IT Ultrastab

Closed-Loop Fluxgate Current Measurement Systems

Very High-Accuracy Current or Voltage Output Signal with Electrical Isolation from the Primary Circuit

Optional Heads	600A	2,000A	5,000A
Lowest fs Current	40A	125A	2,500A
fs Current Range Increment	20A	125A	125A

Very High-accuracy Calibration and Power Measurements

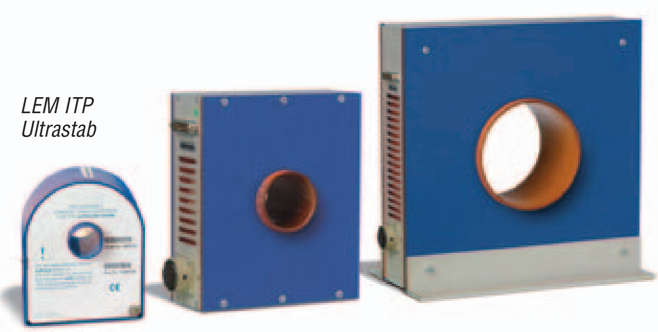

LEM ITP Ultrastab

CALENDAR

SEMINARS: Electrical

Mar 19-21 Instrumentation for Test & Measurement. Las Vegas, NV. Technology Training Inc., http://www.ttiedu.com/schedule.html.

Mar 12-15 MET-101 Basic Hands-on Metrology. Seattle, WA. Fluke Calibration, http://us.flukecal.com/training.

Apr 23-26 MET-301 Advanced Hands-on Metrology. Seattle, WA. Fluke Calibration, http://us.flukecal.com/training.

May 21-23 Instrumentation for Electrical Test & Measurement. Las Vegas, NV. Technology Training Inc., http://www.ttiedu.com/schedule.html.

Jun 4-7 MET-101 Basic Hands-on Metrology. Seattle, WA. Fluke Calibration, http://us.flukecal.com/training.

Jun 12-14 MET-302 Introduction to Measurement Uncertainty. Seattle, WA. Fluke Calibration, http://us.flukecal.com/training.

Jun 25-29 Grounding, Shielding and Test Procedures for EMI/EMC/ESD. Las Vegas, NV. echnology Training Inc., http://www.ttiedu.com/schedule.html.

SEMINARS: Flow & Pressure

Feb 20-23 Comprehensive Hydrocarbon Measurement Training Course. Kuala Lumpur. Colorado Engineering Experiment Station Inc., www.ceesi.com.

Feb 27 Fundamentals of Ultrasonic Flowmeters Training Course. Kuala Lumpur. Colorado Engineering Experiment Station Inc., www.ceesi.com.

SEMINARS: General

Apr 23-27 Fundamentals of Metrology. Gaithersburg, MD. Sponsored by NIST Office of Weights and Measures. http://www.nist.gov/pml/wmd/5163.cfm.

Apr 30-May 1 Metrology Concepts. Las Vegas, NV. Technology Training Inc., http://www.ttiedu.com/schedule.html.

Aug 20 - 24 Fundamentals of Metrology. Gaithersburg, MD. Sponsored by NIST Office of Weights and Measures. http://www.nist.gov/pml/wmd/5179.cfm.

SEMINARS: Industry Standards

Feb 22-24 ISO 17025 Compliance and Auditing Techniques Including ANSI Z540.3 Req's. Orlando, FL. WorkPlace Training, http://wptraining.com/ .

CALENDAR

Feb 28-Mar 1 Cal Lab Management; Beyond 17025 Training. Orlando, FL. WorkPlace Training, http://wptraining.com/ .

Jun 12-14 Cal Lab Management; Beyond 17025 Training. Minneapolis, MN. WorkPlace Training, http://wptraining.com/ .

SEMINARS: Mass & Weight

Feb 27 - Mar 9 Mass Metrology Seminar. Gaithersburg, MD. Two-week seminar, sponsored by NIST Office of Weights and Measures. http://www.nist.gov/pml/wmd/5165.cfm.

May 7-18 Mass Metrology Seminar. Gaithersburg, MD. Two-week, "hands-on" seminar, sponsored by NIST Office of Weights and Measures. http://www.nist.gov/pml/wmd/5166.cfm.

Oct 15 - 26 Mass Seminar. Gaithersburg, MD. Two-week, "hands-on" seminar, sponsored by NIST Office of Weights and Measures. http://www.nist.gov/pml/wmd/5192.cfm

SEMINARS: Measurement Uncertainty

Mar 20-22 Measurement Uncertainty Workshop. Fenton, MI. Presented by QUAMETEC Institute of Measurement Technology, http://www.QIMTonline.com, click on Public/Private Measurement Uncertainty Workshop/Classes.

May 15-17 Measurement Uncertainty Workshop. Fenton, MI. Presented by QUAMETEC Institute of Measurement Technology, http://www.QIMTonline.com, click on Public/Private Measurement Uncertainty Workshop/Classes.

SEMINARS: Pressure & Flow

Apr 16-20 Advanced Piston Gauge Metrology. Phoenix, AZ. Fluke Calibration, http://us.flukecal.com/training.

SEMINARS: Radiometry

Apr 17-20 Spectroradiometry Short Course. NIST Gaithersburg, MD. Offered every 2 years, this 4-day course consists of lectures and hands-on lab experience. http://www.nist.gov/pml/div685/sc/index.cfm.

SEMINARS: Temperature

May 15-17 Temperature Calibration Product Training. American Fork, UT. Fluke Calibration, http://us.flukecal.com/training.

Jun 4-8 Radiation Thermometry Short Course. NIST Gaithersburg, MD. 5-day course consists of lectures and hands-on laboratory experiments. http://www.nist.gov/pml/div685/sc/index.cfm.

Jun 12-14 Principles of Temperature Metrology. American Fork, UT. Fluke Calibration, http://us.flukecal.com/training.

Aug 21-23 Infrared Temperature Metrology. American Fork, UT. Fluke Calibration, http://us.flukecal.com/training.

Sep 18-19 ITS-90 Fixed-Point Cell Mini-Workshop. NIST Gaithersburg, MD. http://www.nist.gov/pml/div685/sc/index.cfm.

Sep 18-20 Advanced Topics in Temperature Metrology. American Fork, UT. Fluke Calibration, http://us.flukecal.com/training.

Sep 19-20 Selecting and Using Alternative Thermometers Mini-Workshop . NIST Gaithersburg, MD. http://www.nist.gov/pml/div685/sc/index.cfm.

SEMINARS: Vibration

Mar 5-8 Fundamentals of Vibration for Test & Design Applications. Las Vegas, NV. http://www.ttiedu.com/schedule.html

May 30-Jun 1 Fundamentals of Vibration for Test Applications. Las Vegas, NV. http://www.ttiedu.com/schedule.html

---

Visit **www.callabmag.com** for upcoming and future events!

Redefining the SI Base Units

Metrology is poised to undergo a profound change that will benefit scientists, engineers, industry and commerce – but which almost no one will notice in daily life.

The international General Conference on Weights and Measures (CGPM) has approved a plan to redefine four of the seven base units of the International System of Units (SI) in terms of fixed values of natural constants. The initiative would make possible new worldwide levels of consistency and accuracy, simplify and normalize the unit definitions, and liberate the system from dependence on the prototype kilogram, an artifact adopted in 1889 and still used as the world's physical standard for mass.

On Oct. 21, 2011, CGPM, the diplomatic body that has the authority under the Meter Convention to enact such a sweeping change, passed a resolution declaring that the kilogram, the ampere, the kelvin and the mole, "will be redefined in terms of invariants of nature; the new definitions will be based on fixed numerical values of the Planck constant (h), the elementary charge (e), the Boltzmann constant (k), and the Avogadro constant (N_A), respectively."

That action follows – and results directly from – decades of pioneering metrology research around the globe, some of it accomplished by various groups at NIST and its antecedent, the National Bureau of Standards (NBS), that are now part of PML. And it echoes the recommendations made by three PML scientists and two European colleagues in an influential 2006 paper in *Metrologia*.

The change1 will not be implemented until the technical requirements for agreement and uncertainties are met. (The next scheduled meeting of the CGPM is in 2014.) In the interim, more work will be required: CGPM has called for further reductions in measurement uncertainty before the "New SI" can be implemented, and encouraged national metrology institutes (NMIs) and other institutions to "maintain their efforts towards the experimental determination of the fundamental constants h, e, k and N_A."

The central philosophy of the impending redefinition is that instead of defining an SI unit per se, the CGPM will specify exact values value for a set of fundamental constants which will set the scale for the SI units. The values of those physical constants will reflect the most accurate determinations available from NIST, NMIs, and academic institutions at the time of implementation.

Three decades ago, the same schema was used for the first time to redefine the meter: In 1983, CGPM defined the meter by setting an exact fixed value of the speed of light in vacuum (299 792 458 m s^{-1}), citing "the excellent agreement among the results of wavelength measurements on the radiations of lasers . . . ."

The meter redefinition relied heavily on a then-new method, devised by NBS researchers in Boulder, to measure the speed of light, and since then PML has been substantially involved in all aspects of the "New SI." In particular, PML groups have made major, sustained contributions to the impending redefinitions of the kilogram and the kelvin, the implementation of which will take place under the auspices of the International Bureau of Weights and Measures (BIPM), an intergovernmental organization under the authority of the CGPM.

NOTE: During 2012, PML at Work will feature a series of articles describing NIST research efforts related to each of the SI base units. These will be posted to http://nist.gov/pml/newsletter/index.cfm.

[1] In February 2012, NIST/PML and NRC Canada will sponsor a special session on SI redefinition at the annual meeting of the American Association for the Advancement of Science.

[2] Other NIST divisions have related research programs.

Source: NIST PML Newsletter (11/2/2011), http://www.nist.gov/pml/newsletter/siredef.cfm.

Penny Calibration

The camera at the end of the robotic arm on NASA's Mars rover Curiosity has its own calibration target, a smartphone-size plaque that looks like an eye chart supplemented with color chips and an attached penny. When Curiosity lands on Mars in August, researchers will use this calibration target to test performance of the rover's Mars Hand Lens Imager, or MAHLI. MAHLI's close-up inspections of Martian rocks and soil will show details so tiny, the calibration target includes reference lines finer than a human hair. This camera can also focus on any target from about a finger's-width away to the horizon.

Curiosity, the rover of NASA's Mars Science Laboratory mission, also carries four other science cameras and a dozen black-and-white engineering cameras, plus other research instruments. The spacecraft, launched Nov. 26, 2011, will deliver Curiosity to a landing site inside Mars' Gale Crater in August to begin a two-year investigation of whether that area has ever offered an environment favorable for microbial life.

The "hand lens" in MAHLI's name refers to field geologists' practice of carrying a hand lens for close inspection of rocks they find. When shooting photos in the field, geologists use various calibration methods.

MAHLI Principal Investigator Ken Edgett, of Malin Space Science Systems, San Diego, bought the special penny that's aboard Curiosity with funds from his own pocket. It is a 1909 "VDB" cent, from the first year Lincoln pennies were minted, the centennial of Abraham Lincoln's birth, with the VDB initials of the coin's designer - Victor David Brenner -- on the reverse.

"The penny is on the MAHLI calibration target as a tip of the hat to geologists' informal practice of placing a coin or other object of known scale in their photographs. A more formal practice is to use an object with scale marked in millimeters, centimeters or meters," Edgett said. "Of course, this penny can't be moved around and placed in MAHLI images; it stays affixed to the rover."

The middle of the target offers a marked scale of black bars in a range of labeled sizes. While the scale will not appear in photos MAHLI takes of Martian rocks, knowing the distance from the camera to a rock target will allow scientists to correlate calibration images to each investigation image.

The Mars Science Laboratory is managed by NASA's Jet Propulsion Laboratory, a division of the Caltech. For more information, visit http://www.nasa.gov/msl .

Source: http://www.jpl.nasa.gov/news/news.cfm?release=2012-033.

Quantum-Based Impedance Bridges

Traditional impedance bridges make use of inductive dividers and achieve, in their frequency range from 500 Hz to 10 kHz, excellent relative measurement uncertainties of only a few parts in 10^{-9}. The bridges must, however, be adjusted for each frequency of operation and this involves a complex manual procedure.

PTB's newly developed Josephson Impedance Bridge can be adjusted very easily. The AC voltage amplitudes from two Josephson arrays are adjusted over their microwave frequency, and the phase angle between the synthesized voltages is adjusted via delay electronics with a resolution of 10 ps. Both processes are fully automatic. The utilization of quantum standards to generate a voltage on both sides of the bridge renders new adjustments at all other frequencies unnecessary. It is therefore possible to perform precise measurements at 20 different frequencies within just 30 minutes.

The efficiency of the new procedure has been demonstrated by measuring the 1:1 ratio between two 10 kΩ resistors and two 100 pF capacitors. The resistance ratio over the frequency range from 25 Hz to 10 kHz was determined with a measurement uncertainty of approx. $2 \cdot 10^{-8}$. For capacitance ratios, the uncertainty lies in the kHz range below $1 \cdot 10^{-8}$. With decreasing frequency, the uncertainty increases as a function of the impedance $1/\omega C$. With $2 \cdot 10^{-7}$ at 25 Hz, the uncertainty is, however, still 20 times smaller than when measuring with traditional bridges.

In further development steps, the new Josephson Bridge is to be used also for ratio measurements where a resistor is compared to a capacitor. By integrating the frequency-independent quantum Hall resistor, the frequency response of capacitors could then be calibrated up to the range of technical with high precision.

Source: PTB News 2/2011, http://www.ptb.de/.

QuadTech Acquired by Chroma Systems Solutions

Chroma Systems Solutions, Inc. (CSS) announced today the acquisition of primary assets of Massachusetts-based QuadTech, Inc., an industry-leading provider of electrical safety equipment and systems. CSS, located in Southern California, is a complete solutions provider of power electronics testing instrumentation and systems. Under Chroma's ownership, QuadTech customers will benefit from an increased product offering and power testing expertise as well as more access to inventory, applications, services and world-class customer support.

Established more than 20 years ago, QuadTech achieved strong business growth and forged strong relationships with their customer base distributing products manufactured by Chroma under their brand. QuadTech, which now will operate entirely under the Chroma brand, will be led by Chroma Systems Solutions' President and CEO, Fred Sabatine.

With this acquisition, QuadTech employees join Chroma Systems Solutions in providing sales and service of Chroma's comprehensive line of electrical power test instrumentation and automated test systems as well as safety testers throughout North American including new products targeted at emerging commercial and defense markets, solar, EV/Automotive and LED.

Chroma Systems Solutions, Inc. is the North American business unit of Chroma ATE, the world leader in power testing instruments and systems. For more company and product information visit www.chromausa.com.

New *GAGEpack* Release

A new release of GAGEpack from PQ Systems features more efficient drag-and-drop label actions, automatic recording of temperature-humidity USB module (THUM) data, and additional options for visual styles. An improved, flexible To Do list and daily checks for imminent license expiration are among other highlights offered by the newest release.

GAGEpack is powerful gage calibration software that saves time and enhances accuracy in gage management and measurement systems analysis. It maintains complete histories of measurement devices, instruments, and gages. To ensure timely calibration, the software provides a variety of tools, such as:

- Calibration schedules and reports
- Alerts about failed and past due calibrations
- Gage location and status tracking
- Gage repair records
- Audit trail for traceability
- A Task tab with a To-Do list

The To Do list in the newest release indicates items requiring attention for a user-selected period of time. The list can be filtered by action and ordered with a simple click of column headers, and can be sent via email to designated receivers. New columns can be created with just a click to enhance task management and save time.

If a THUM is connected, *GAGEpack* will automatically record the temperature and humidity for a new calibration or verification event, providing critical information at one's fingertips.

GAGEpack 9.5, like its predecessor, is a .NET program, so it will continue to evolve and improve using the newest available technology, according to lead program developer Jeff Aughton. Current users will find the transition to the new release seamless, he adds.

For more information: http://www.pqsystems.com/.

Palmer Instruments, Inc. Transducers

Celebrating 176 years of temperature and pressure expertise in 2012, Palmer Instruments, Inc. is pleased to announce the introduction of Pressure Transducers to its line of industrial pressure and temperature instrumentation. Choose electrical signal outputs in 4-20 mA, 0-5 V, and 1-10 V with Packard, DINN, or Cable type electrical connections. Available in six different series, Palmer Pressure Transducers feature ceramic, silicone, or piezoresistive sensing elements for excellent linearity and

outstanding inherent reliability. Quality housings of 304 or 316 stainless steel are rugged for long-term use applications in a wide variety of industries, including HVAC, water treatment, hydraulic control and monitoring, compressors, aerospace, and process control.

Accuracies are as precise as 0.2% of Full Scale, with maximum ranges of 8700 PSI available on some models. Work with our in-house engineers to design custom configurations to meet the needs of your application.

Pressure transducers are available through Palmer Instruments, Inc. and its International Distribution network. For additional information please contact us at sales@palmerwahl.com or call 1-800-421-2853.

Modal Shop SmartShaker™ & SmartAmp™

The Modal Shop's line of modal exciters and vibration shakers is available standard as complete turnkey systems to serve your testing needs. With models ranging from 4 lbf (20 N) to 110 lbf (489 N), you can find the right shaker for your modal or vibration study. Available designs include the revolutionary new SmartShaker™ with integrated power amplifier, a variety of mini, through-hole modal exciters, platform vibration shakers and the new SmartAmp™ power amplifiers. A graphical selection guide is available at www.modalshop.com/excitation.

Each exciter includes a trunnion base with ergonomic EasyTurnTM handles to make adjusting shaker position and alignment simple. The exciter is also accompanied by all the necessary cables and a companion amplifier. Accessory kits include stingers in various sizes, chucks, and collets to make connecting the shaker and test object easy. Also supplied are all the tools needed to help with stinger installation or to add and remove adaptor and mounting inserts. Other accessories include spare fuses, low profile trunnion bolts and adaptors to help meet requirements for many different application setups.

The Modal Shop, Inc. offers many unique sound and vibration testing products and accessories. For specification sheets, application data and pricing, please contact THE MODAL SHOP, INC., 3149 E. Kemper Road, Cincinnati, OH 45241-1516, Internet: www.modalshop.com, 800-860-4867, Fax 513-458-2172 or e-mail: info@modalshop.com.

Mitutoyo 0.1µm Micrometer

Mitutoyo America Corporation announces availability of its new, High-Accuracy Digimatic® Digital Micrometer – the first micrometer to offer 0.1µm The High-Accuracy Digimatic® Micrometer utilizes the Absolute® rotary sensor (patent pending) manufactured utilizing Mitutoyo's own high precision screw machining technology. This sensor reduces instrument error to ±0.5µm to deliver high-accuracy with no trade-off in operability. The Absolute® system eliminates the need to reset the origin each time power is turned on thus enabling measurement immediately upon start-up.

The Mitutoyo High-Accuracy Digimatic® Micrometer features an extremely rigid frame for stable measurement while a constant-force barrel/spindle mechanism eliminates the possibility of overspeed errors. Additionally, the Mitutoyo High-Accuracy Digimatic® Micrometer supports output to measurement data applications such as MeasurLink®, Mitutoyo's proprietary statistical-processing and process-control program which performs statistical analysis and provides real-time display of measurement results for SPC applications.

Mitutoyo's nationwide network of Metrology Centers and support operations provides application, calibration, service, repair and educational programs to ensure that our 6,000+ metrology products will deliver measurement solutions for our customers throughout their lifetime. Contact Mitutoyo America Corporation, 965 Corporate Boulevard, Aurora, IL 60502. Phone: (630) 820-9666. E-mail: info@mitutoyo.com. http://www.mitutoyo.com.

On Time Support METEX2 & Email Notification – New Version Release

On Time Support, Inc., based in Spring, Texas, has released new versions of Metrology Xplorer 2 (METEX2 version 250+) and their popular Email Notification product (version 250+).

METEX2 is a browser product compatible with the Fluke® Calibration's MET/TRACK® product. METEX2 allows complete browser operation of MET/TRACK® without the installation process, including Crystal Reports. Managers and users can always have access to the MET/TRACK® database. METEX2 also performs very well over WAN installations. Based on On Time Support's METDaemon technology, METEX2 provides the customer with the ultimate in browser technology. On Time Support has been providing browser products for MET/TRACK® since 1999. Demonstration packages are available.

Email Notification allows users to schedule automatic email deliveries of various metrology activities to customers or other personnel. Based on On Time Support's METDaemon technology, administration is performed via a browser with no client installation. New Dynamic Email options and delivery confirmations provide the busy manager with multiple options when sending automated emails. When combined with the new METDaemon Responder, customers can respond back directly to the database.

More information on METEX2 & Email Notification is available at www.ontimesupport.com. Contact On Time Support at inquiries@ontimesupport.com or call 281-296-6066.

Fluke Calibration MET/CAL ® *Plus* Version 8.0

Calibration labs have their share of challenges: an increasing and more complex workload; fewer technicians; a growing list of quality standards. Above all, there's constant pressure to reduce costs.

MET/CAL® *Plus* Version 8.0 Calibration Management Software helps you to meet those challenges by managing and calibrating your workload more efficiently. It includes MET/CAL® – the industry-leading software for automated calibration and MET/TRACK® – a dedicated system to manage your test and measurement assets. MET/CAL® *Plus* software supports the way your lab operates:

- Add new items to MET/TRACK just by typing information into a form.
- Generate recall reports.
- Store all parameters for every calibration test step for future reporting or analysis and a clear audit trail.
- Create and print ad hoc reports in Quick Report Builder or build your own reports using Crystal Reports Professional (included).

With all of these capabilities, MET/CAL® *Plus* offers the most comprehensive calibration automation solution available. And we back it up with MET/SUPPORT Gold plans that help you get up and running and keep you as productive as possible.

What's new in Version 8.0?

- New expanded Procedure Editor with flexible user interface and enhanced functionality
- Increased security for accredited procedures
- Ability to automate a wider variety of references
- Compliance to Z540.3 decision rules by guard banding
- Greater flexibility and expanded support of power meters and sensors
- New LIB FSC that allows procedure access to external programs
- Access to National Instruments DLLS, enabling calibration of PXI instruments with MET/CAL software
- Option to use Excel for customized plotting and calculations
- Linked online help

For more information, visit: http://www.flukecal.com.

Vaisala Humidity and Temperature Transmitter Series

Vaisala introduces the next generation of humidity and temperature transmitters for demanding HVAC applications. Combining fit with functionality, the new Vaisala HMW90 Series HUMICAP® Humidity and Temperature Transmitters are designed for indoor environments requiring measurement accuracy and stability that can be depended on.

The Vaisala HMW90 Series comprises wall-mounted humidity and temperature transmitters with a variety of options and features, including special scalings and calculated dew point and mixing ratio parameters. Vaisala's proven HUMICAP® 180R humidity sensor technology, now introduced to HVAC transmitters, guarantees highly accurate measurements and long-term reliability, while innovative design makes the transmitters easy to install, use and calibrate.

For fast and convenient maintenance, the transmitters include an instructive display, which can be hidden behind a solid cover. The front cover slides down, which means that calibration and adjustment interfaces are within easy access without disturbing measurement performance. For field adjustment, all it takes is a screwdriver and a reference instrument - no special tools or software are needed.

For more information, visit: http://ww.vaisala.com/hmw90.

Finally… A Humidity Generator that Stabilizes in less than 5 minutes, has the Capacity to Calibrate 12 Probes and can Complete a 3 Point RH Calibration of Chart Recorders with Embedded Sensors in 60 minutes… Automatically!!!

The M2000SP-XR Humidity Generator

One System…Three Functions

High Accuracy Calibration of Instruments

The field proven M2000SP-XR with new solid state electronics for high accuracy and performance over the full operating range of humidity and temperature. The temperature compensated control probe provides higher accuracy over the range of measurement. Newly designed electronics is incorporated within the heat/cool circuitry and a more efficient peltier mechanism, has been incorporated for faster response and temperature stability. The number of ports in the chamber door has been increased to accept 5 probes with diameters of 10mm, 12mm, 15mm and 18mm. NVLAP Accredited calibration of control probe. System tested for performance at ICH guideline parameters to meet accuracy and long term stability requirements. Typical response time is 3 minutes for 70%RH step change.

Production and Volume Calibrations at Ambient Temperature

The chamber size of the M2000SP standard system is 2 liters. For calibrations of multiple data loggers or sensors the chamber capacity must be increased. The M2000SP-XR, using the 12 port external chamber, provides the increased calibration capabilities through the use of a chamber with internal dimensions of 250mm x 200mm x 100mm (h x w x d). Nine (9) horizontal ports have sufficient separation to prevent interference and to maximize number of transmitters for insertion within the chamber. Three (3) top ports are for instruments with long probes (250mm) or reference standards to verify internal readings. Clear chamber door for visual observation of instruments with digital displays.

Calibration of Chart Recorders with Embedded Sensors Using Programmed Procedures

For fast, accurate calibration of battery operated chart recorders having the RH/T sensors embedded within the recorder housing. The internal blower of the M2000SP has been modified for a more efficient air flow, both within the internal chamber and the external chambers. The large external chamber has internal dimensions of 300mm x 250mm x 150mm (h x w x d). Accurate RH calibrations over the range of 10-90%RH, at ambient temperature, can be done more quickly than when using larger chambers. A typical 3 point RH calibration can be done in less than 1 hour after temperature has stabilization. The internal chamber conditions are verified using a reference instrument calibrated by an NVLAP Accredited laboratory according to ISO/IEC guidelines and 17025 procedures. Through the use of pre-programmed calibration procedures, the required calibration cycle can be done automatically.

Tel: (631) 951-9100 **Kaymont Consolidated Industries** **Fax: (631) 951-9109**

180 Oser Avenue, Suite 200, Hauppauge, NY 11788

ThermoProbe TL2 Digital Reference Thermometer

ThermoProbe, Inc., a company with a long history in the design and manufacture of digital thermometers for use in petrochemical storage facilities, refineries, explosive environments, laboratories, and other specialized temperature measurement fields, is pleased to introduce the new ThermoProbe TL2, the newest technology in non-mercury reference thermometers,

The TL2 is built on technology proven by several thousand field-tested TL1 models, and represents the latest in thermometer design. The TL2 is a 2-channel, precision bench-top platinum resistance thermometer (PRT) offering a higher level of metrology accuracy than mercury thermometers and most digital thermometers. Ready to use, right out of the box, the TL2 comes as a conveniently packaged instrument with exchangeable sensor(s), calibrated as a complete NIST-traceable thermometry system. It's also cost-effective, which -- as every lab manager knows -- is not always the case with new technologies. In addition to being a reference thermometer, the TL2 provides easy to use data logging capabilities with the convenience of PC- or USB-flash drive interface.

Several states now prohibit the sale of mercury-containing thermometers. The National Institute of Standards and Technology ceased calibrating mercury-in-glass thermometers for traceability purposes in March 2011 and is working with EPA, ASTM, and API to seek out viable alternatives.

The ergonomic design and large display make the TL2 ideally suited for use as a calibration reference thermometer and for recording temperature-time based data. Using dual channels, the TL2 provides data logging capabilities for two simultaneous measurements with the convenience of PC- or USB-flash drive interface. Users can download data from the TL2 using its flash drive port and upload directly onto a PC. Unlike most comparable devices, the TL2 does not require the purchase of separate digital readout and probe sensors. There is no need to send two separate components to a calibration lab to get the unit up and running. Just open the box, plug it in, and start taking your calibrated measurements.

For more information, visit: http://www.thermoprobe.net.

Gooch & Housego OL 730E Radiometer/Photometer

After many years of success and proven performance with our OL 730C, Gooch & Housego announces the release of the OL 730E Radiometer/Photometer.

This newest model in the OL Series 730 line boasts a smaller footprint and reduced cost while providing similar research-grade precision and accuracy. The OL 730E has an internal preamplifier and a sensitivity of 1 X 10^{-14} amperes. It may be virtually controlled via the USB interface, and boasts a response time as fast as 0.1 seconds and a full-scale range of 2 x 10^{-10} to 2 x 10^{-3} amperes.

Also being offered with this new radiometer will be a series of TE-cooled detectors, which will provide enhanced temperature stability over time while utilizing a smaller control unit.

For more information, visit: www.goochandhousego.com/products/systems.

Agilent Technologies New Wireless Communications Test Set

Agilent Technologies Inc. announced the new E5515E 8960 Series 10 wireless communications test set, designed for R&D engineers who need to stress their 2G/3G/3.5G designs at the maximum data rates.

The E5515E, an enhancement to the industry-preferred 8960 wireless test set, is equipped with dual downlink paths, a more powerful processor and other significant hardware improvements. It includes advanced features such as sustained 42-Mb/sec DCHSDPA throughput and extensive handovers between 2G/3G and LTE, for comprehensive 2G/3G/3.5G/LTE testing together with the Agilent PXT E6621A wireless communication test set for LTE. In addition, the E5515E wireless test set supports the latest TDSCDMA advancements such as TDHSDPA 2.8-Mb/sec IP data connections, TDHSUPA signaling and test-mode connections, and TDSCDMA protocol logging.

The E5515E wireless test set complements the currently available E5515C, which continues to offer robust, repeatable and standards-compliant 2G/3G/3.5G RF measurements for both R&D and manufacturing. Existing E5515C test sets can be upgraded to E5515E hardware to support the latest 3.5G technologies such as 42-Mb/sec DCHSDPA.

For more information, visit: http://www.agilent.com/find/E5515E.

Calibrating 1 mW 50 MHz Power Reference Output

By Hock Eng Lim
Agilent Technologies

Part I

Introduction

Measuring or verifying the 1 mW (0 dBm) 50 MHz power reference is one of the key tasks when doing the annual service or calibration on RF power meters. In calibration laboratories or service facilities, engineers and technicians have been calibrating and measuring the power reference in order to maintain the power meter's measurement accuracy. In other words, maintaining the accuracy and traceability of the power reference indirectly minimizes the power meter's measurement uncertainty.

All existing RF power meters have the power reference output (source) or, sometimes simply called, the reference calibrator (see Figure 1). Prior to performing any direct power measurement using a power meter and sensor, zero and calibration has to be done to ensure the power measurement will be accurate. The power sensor has to be connected to the power reference source so that all the calibration factor corrections done within the power meter (connected with a power sensor) are referenced to the 1 mW 50 MHz source.

The 1 mW power reference source typically has a very tight specification, in the range of ± 0.5% to 0.9%. Hence, in order to measure the power reference, a higher accuracy power meter and sensor, such as the thermistor mount power meter, is to be used [1].

This article explains the application procedure on how to measure and calibrate the power reference of power meters. There will be a step by step on how to perform the measurement using a thermistor power meter, followed by the measurement uncertainty or expected measurement error, a basic statistical way of obtaining the total measurement uncertainty. We will be using the Agilent N432A Power Meter pictures and uncertainty models in our example.

Measurement Setup for the 1 mW 50 MHz Power Reference Measurement

A typical measurement setup example for measuring the reference calibrators using the thermistor power meter is show in Figure 2. The thermistor power meter illustrated here is the Agilent's N432A [5]. The 3458A Digital Multimeters (DMMs) are used to measure the DC output voltages (V_{COMP} and V_{RF}) of the thermistor power meter [3]. This setup is widely used by the calibration or metrology labs because of the superior accuracy and traceability.

Specially made thermistor mounts (Figure 3) are used when performing power reference measurement which has a very low mismatch or standing wave ratio (SWR) at 50 MHz. The reason for having low SWR at 50 MHz is to reduce the mismatch measurement uncertainty or errors when these mounts are connected to the reference calibrator of the power meters under test. From past experience, mismatch errors can significantly impact the overall measurement uncertainty. A good example of such special mounts is Agilent's 478A option H75 or H76 and 8478B option H01. These mounts are made to have SWR less than 1.05 at 50 MHz, compared to normal mounts which can be have SWR of 1.3 typically.

Figure 1. 1 mW (0 dBm) 50 MHz power reference calibrator on power meters.

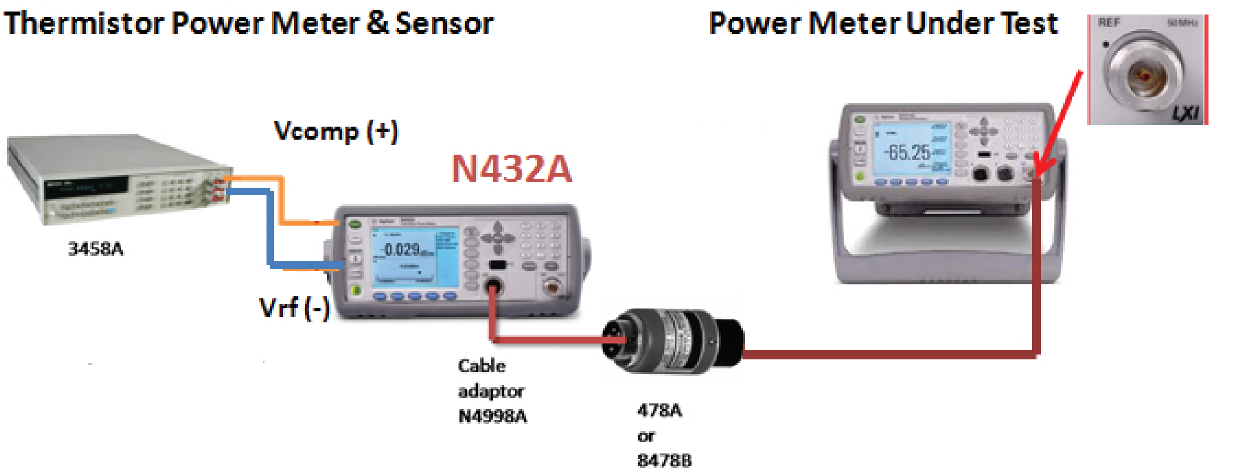

Figure 2. 1 mW 50 MHz Power Reference Measurement setup.

Part II

Power Reference Measurement Procedures

1. Connect the equipment as shown in Figure 2.
2. Set the 3458A DMM to measure DCV.
3. Ensure that the N432A and the power meter under-test have been powered on for at least 30 minutes before continuing, recommended warm up time.
4. Zero set the N432A; make sure the power reference of the power meter under test is turned off.
5. Round the DMM reading to two decimal places and record this reading as V_0 .This is the voltage measured between V_{COMP} and V_{RF} connectors when no RF power is applied (the calibrator reference is turned off).
6. Turn on the power reference on the power meter under test.
7. Round the DMM reading to two decimal places and record this reading as V_1 (typically about 80 mV). In other words, V_1 is the voltage measured between V_{COMP} and V_{RF} connectors when the calibrator reference power is turned on.
8. Disconnect the DMM negative input lead from the VRF connector on the N432A and connect it to the N432A chassis ground.
9. Record the reading DMM result as V_{COMP} (typically about 4.8V). V_{COMP} is the voltage of the temperature compensated bridge.
10. Calculate the Power Reference Oscillator power using Equation 1. The value for R can be set as 200Ω typical. The CF is the calibration factor for the thermistor mount at 50 MHz, typically set as 99%.
11. The expected power measurement results (calculated) should be 1 mW ± 0.9% [4].

$$P = \frac{2V_{comp}(V_1 - V_0) + V^2{}_0 - V^2{}_1}{4 \times R \times CF} \quad (1)$$

Figure 3. Special tuned low SWR at 50 MHz thermistor mounts.

Uncertainty Contributors	Units	Value	± Limits	Uncertainty Contributed (Standard Uncertainty x Sensitivity)
Voltage measurement for Vcomp	V	4.8	0.00003845	4.67×10^{-9}
Voltage measurement for V1	V	0.080	0.00000098	6.77×10^{-9}
Voltage measurement for V0	V	0.0023	0.00000032	-2.23×10^{-9}
Bridge resistance measurement, R	Ω	200	0.00250	-7.35×10^{-9}
CF (Calibration Factor)	Ratio	0.99	0.004 (calibrated by standard lab)	-2.06×10^{-6}
M (Mismatch Uncertainty)	Ratio	1.00	0.00142 ($2 \times \Gamma_s \times \Gamma_d$)	-1.02×10^{-6}

Root Sum Square	2.29×10^{-6}
Coverage Factor, k=2 for 95% confidence	2
Expanded Uncertainty	4.59×10^{-6}
Expanded Uncertainty in % for 1 mW	**0.4597**

Table 1. Measurement Uncertainty Budget Table.

Part III

Power Measurement Uncertainty Equation

The measurement uncertainties for measuring the 1 mW reference calibrators will be based on the power measurement Equation 2 below [4]. The equation is a modified version of Equation 1 to include the mismatch term (M) to account for the non perfect power transfer from the power reference (power meter under test) to the thermistor mount.

$$P = \frac{2V_{comp}(V_1 - V_0) + V^2{}_0 - V^2{}_1}{4 \times R \times CF \times M} \quad (2)$$

M is the maximum (worst case) mismatch uncertainty between the calibrator reference to be measured and the thermistor mounts connector. It takes the form ($1+/- 2\Gamma_s \times \Gamma_d$), where Γ_s is the power reference reflection coefficient and Γ_d is thermistor mount reflection coefficient.

Power Measurement Uncertainty Model Assessment

Typically the power measurement uncertainty assessment is obtained using the uncertainty tabulated budget model. The assessment starts by collecting all the uncertainty contributors, for this case they are V_{COMP}, V_0, V_1, R, CF, and M. Each contributor will then to be derived and then root sum square them together, this is called the RSS method. Table 1 is a worked example of the 1 mW power reference measurement uncertainty based on set up shown in Figure 2 previously. The content has been simplified and only to show at the end, the individual contributions of each parameters in Equation 2. Please refer to Agilent's Application Note 1449-3 [2] for details. The result shows the total measurement uncertainty using N432A thermistor power meter and sensor is 0.46%.

Conclusion

Over the years, thermistor based power meter has been used to measure and calibrate the 1 mW 50 MHz power reference calibrator of RF power meters because of its high accuracy, reliability and traceability to standard labs. As shown in the power measurement uncertainty example, these power meters (with special thermistor mount) provides a very low uncertainty which is around 0.5%. From the worked example shown, it is clear that the two most significant contributors are the mismatch error and the CF uncertainty. Hence, to maintain low mismatch uncertainty, a super low reflection coefficient themistor sensor is to be used. As for the CF uncertainty, one way is to make sure the sensor is calibrated at a standard metrology lab to maintain great consistency, low uncertainty, and minimum drift.

References

[1] Radio Frequency & Microwave Power Measurement, Alan Fantom, IEEE.

[2] "Agilent Fundamentals of RF and Microwave Power Measurements," Application Note 1449-3.

[3] “Measuring RF Power” by Joe Carr. Electronic World November 1999.

[4] Agilent EPM-P E4416/17A Service Guide.

[5] Agilent N432A Thermistor Power Meter User Guide.

Hock Eng Lim, Agilent Technologies, hock-eng_lim@agilent.com.

Comparison of Uncertainty Calculation Models

Hening Huang
Teledyne RD Instruments

Three models are available in the literature for calculating the expanded uncertainty using the experimental standard deviation: the Student's *t* model, Craig model, and Bayesian model. This paper compares these three models by Monte Carlo simulation and by examining the random error and bias of the calculated expanded uncertainty. The results indicate that, among the three models, the Student's *t* model is the least precise and accurate, the Craig model is more precise and accurate than the Student's *t* model, and the Bayesian model is the most precise and accurate because of its use of prior information. When prior information is available, the Bayesian model is preferred for calculating the expanded uncertainty. When prior information is not available, the Craig model is preferred.

Introduction

Consider the Type A evaluation of uncertainty in measurements. We assume the population of the measurand (denoted as $\bar{q}$) exists and is normally distributed with a mean, μ, and standard deviation, σ, which, we may not know. The mean of n independent observations of the measurand (denoted as $\bar{q}$) is an estimate of the true mean. We can say that the true uncertainty of $\bar{q}$ exists, whether or not we know it. When the population standard deviation is known, the true uncertainty U at the 95% confidence level (the 95% confidence level is used throughout this paper) associated with $\bar{q}$ can be calculated as

$$U = z_{95}\ \sigma[\bar{q}] = z_{95}\ \frac{\sigma[q]}{\sqrt{n}}\ , \quad (1)$$

where z_{95} is the coverage factor for the 95% confidence level from the normal distribution. It is the 95th percentile point for the two-tailed normal distribution. The parameter $\sigma[\bar{q}]$ is the population standard deviation of $\bar{q}$, and $\sigma[q]$ is the population standard deviation of q. Note that $\sigma[\bar{q}] = \sigma[q]/\sqrt{n}$ is the true standard uncertainty. Eq. (1) was originally developed in the 19th century and was based on the Law of Probability of Errors (e.g., Airy 1861), though U was called the "probable error of the mean" at that time.

In practice, we often have a limited number of observations without knowing the population standard deviation. In this situation, the experimental standard uncertainty, $s[\bar{q}]$, is used as an estimate of $\sigma[\bar{q}]$, and z_{95} is replaced by a coverage factor k in Eq. (1) (e.g., ISO-GUM 1993)

$$U_s = k\ s[\bar{q}] = k\ \frac{s[q]}{\sqrt{n}}\ , \quad (2)$$

where U_s is the expanded uncertainty estimated using the experimental standard deviation $s[q]$. Note that hereafter, $s[\ ]$ means experimental standard deviation for the random variable in [ ], and $\sigma[\ ]$ means population standard deviation.

Three models are available in the literature for calculating the expanded uncertainty, U_s, using the experimental standard deviation. They are the Student's *t* model, Craig model, and Bayesian model. Because the experimental standard deviation is a random variable, its use will result in uncertainty (i.e., random error) in the calculated expanded uncertainty. ISO-GUM (1993) defined the ratio of $\sigma[s[\bar{q}]]/\ \sigma[\bar{q}]$ as a measure of the relative uncertainty of the experimental standard uncertainty $s[\bar{q}]$ and called it the "uncertainty of the uncertainty" of $\bar{q}$. This paper extends the ISO-GUM (1993) discussion and examines the random error of the expanded uncertainty, U_s, calculated by Eq. (2) from the three models. In addition, this paper examines the bias of the calculated uncertainty.

It is assumed that the readers are familiar with the mathematics of modern uncertainty analysis theory. Therefore, this paper will more specfically focus on the precision and accuracy of a model, regardless of how the model is developed.

Uncertainty Calculation Models

Student's t model

The Student's t model is written as

$$U_s = t_{95}\, s[\bar{q}] \,, \tag{3}$$

where t_{95} is the coverage factor with 95% confidence level from the Student's t distribution. It is the 95th percentile point for the two-tailed Student's t distribution (e.g., ISO-GUM 1993).

The Student's t model originated from the work of "Student" (W.S. Gosset) published in 1908 (Student 1908). It is often used when the population standard deviation is unknown and the sample size n<30 (refer to an uncertainty analysis textbook or ISO-GUM 1993). However, Huang (2010) revealed a paradox in measurement uncertainty analysis associated with the Student's t model.

Craig model

The Craig model is written as (Craig 1927, Huang 2010)

$$U_s = \frac{z_{95}}{c_4} s[\bar{q}] \quad , \tag{4}$$

where c_4 is a function of the sample size (e.g., Wadsworth 1989), and

$$c_4 = \sqrt{\frac{2}{N-1}} \frac{\Gamma\left(\frac{N}{2}\right)}{\Gamma\left(\frac{N-1}{2}\right)} \qquad (N=2, 3, \ldots), \tag{5}$$

where $\Gamma(x)$ stands for Gamma function.

Although Eq. (4) was first introduced by Craig in 1927, it is relatively unknown to the measurement uncertainty analysis community. Huang (2010) suggested using the Craig model as an alternative to the Student's t model.

Bayesian model

The Bayesian model is written as

$$U_s = \frac{z_{95}}{\sqrt{1+\frac{1}{\gamma^2}}} s[\bar{q}] \tag{6}$$

or:

$$U_s = \frac{z_{95}}{\sqrt{1+\gamma^2}} s_p[\bar{q}] \quad , \tag{7}$$

where γ is the ratio of the prior standard uncertainty $s_p[\bar{q}]$ to the experimental standard uncertainty $s[\bar{q}]$ of the current measurement (Phillips et al 1998)

$$\gamma = \frac{s_p[\bar{q}]}{s[\bar{q}]} \quad . \tag{8}$$

Eqs. (6) and (7) are derived from the a posteriori standard uncertainty formula presented in Phillips et al (1998) and assume that the coverage factor $k = z_{95}$.

It should be pointed out, unlike the Student's t or Craig model, the uncertainty calculated using the Bayesian model is not associated with the mean of n observations of the current measurement. It is associated with the best estimate of the measurand using prior (historical) information (Phillips et al 1998)

$$q_B = \bar{q}\left(\frac{\gamma^2}{1+\gamma^2}\right) + q_P\left(\frac{1}{1+\gamma^2}\right), \tag{9}$$

where q_B is the best estimate of the measurand with a Bayesian adjustment, and q_P is the best estimate of the measurand based on prior (historical) information.

In addition, note from Eqs. (6) and (7) that, regardless of the value of the ratio γ, the calculated uncertainty will be smaller than either the experimental standard uncertainty or the prior standard uncertainty. That is, "The use of prior information can only decrease the uncertainty associated with the measurand and will never increase it" (Phillips et al 1998).

Monte Carlo Simulation of Uncertainty

In order to understand the random error and bias of the expanded uncertainty calculated by the three models, we first present the results from a Monte Carlo simulation. Assume that the measurement uncertainty (95% confidence level) of a single measurement of water velocity by a water-velocity sensor is 20%, according to the manufacturer's technical specification. On one hand, based on this specification, the true uncertainty of the measurand is 20% for one observation, 14.1% for two, 11.5% for three, and 10% for four. Note that the true uncertainty is the same as the Type B evaluation of uncertainty. On the other hand, if we use the velocity sensor to collect a series of velocity data, we can conduct a Type A evaluation of the uncertainty. Here we consider small samples only (sample size less than 10) and employ a Monte Carlo simulation for the Type A evaluation.

Assume the measured velocity data was normally distributed with a population mean of 20cm/s and standard deviation of 2.04cm/s (derived from the 20% precision specification). The Monte Carlo simulation was conducted using an Excel spread sheet to generate 5000 random numbers (i.e., measured velocities) from the assumed (normal) distribution. Experimental standard deviations were calculated for each observation from n=2 through 10, and expanded uncertainties were then calculated using the Student's t model, Eq. (3), Craig model, Eq. (4), and Bayesian model, Eq. (6). The population standard deviation (2.04cm/s) was assumed to be the prior standard deviation when using the Bayesian model.

Figure 1 shows the scatter plots of relative uncertainty results from the Monte Carlo simulation. To avoid crowding, only the first 200 simulated data points are shown. The relative uncertainty is defined as the ratio of the simulated uncertainty to the true mean velocity (20cm/s). The mean of the simulated uncertainty and the true uncertainty (i.e., the Type B evaluation results) are also shown in the figure.

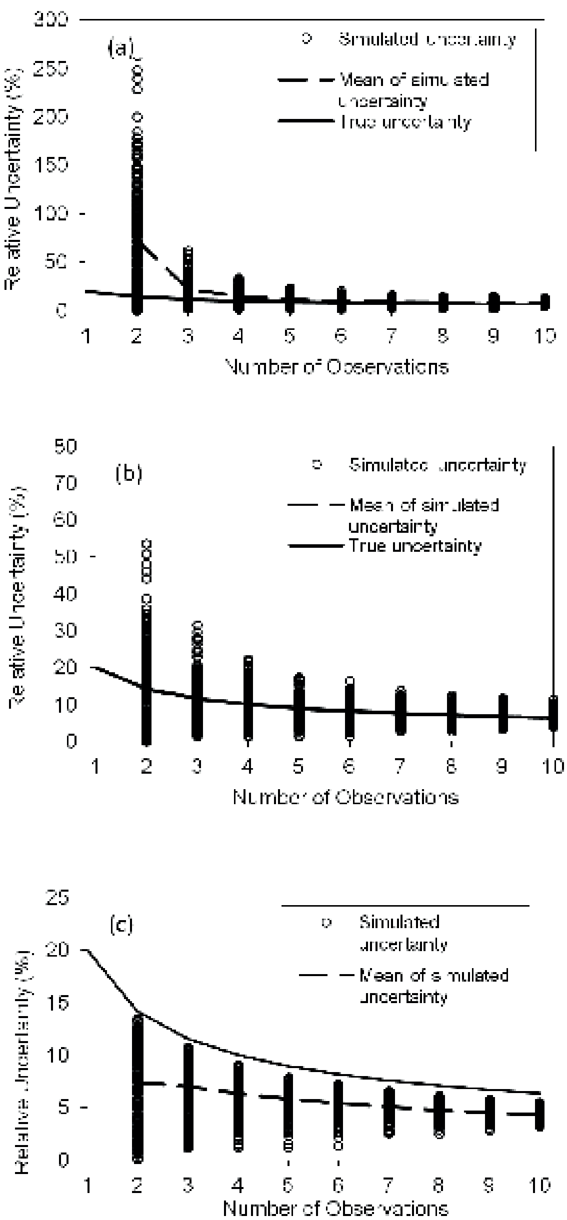

Figure 1. Relative uncertainties from Monte Carlo simulations: (a) Student's *t* model, (b) Craig model, and (c) Bayesian model.

It can be seen from Figure 1 (a) that, for small samples (n<5), the simulated uncertainties from the Student's t model are very scattered and most values are much greater than the true uncertainty. In particular, at n=2, the simulated relative uncertainty ranges from near zero to 250%, while the relative true uncertainty is only 14.1%. This indicates that the Student's *t* model has high random error for small samples. In addition, the mean of the simulated uncertainties significantly deviates from the true uncertainty, indicating that the Student's *t* model has a significant bias from the true uncertainty for small samples.

It can be seen from Figure 1 (b) that the simulated uncertainties from the Craig model are also scattered. But their range is much smaller than that of the Student's *t* model. In addition, the mean of the simulated uncertainties is almost the same as the true uncertainty with only minor errors due to the numerical procedure, indicating that the Craig model has no bias from the true uncertainty.

It can be seen from Figure 1 (c) that the simulated uncertainties from the Bayesian model are the least scattered among the three models. Note that all of the simulated uncertainties are smaller than the true uncertainty. This is expected because the true standard uncertainty is used as the prior standard uncertainty in the Monte Carlo simulation, i.e., $s_P[\bar{q}] = \sigma[\bar{q}]$ in Eq. (6). Thus, no matter what the ratio γ is, the uncertainty calculated using the Bayesian model will be smaller than the true uncertainty. In addition, it is important to note that the true uncertainty is associated with the mean of n observations in the current measurement. It is not the true uncertainty of the measurand with a Bayesian adjustment. The fact that the uncertainty calculated using the Bayesian model is smaller than the true uncertainty means that the measurand with the Bayesian adjustment has a smaller uncertainty than the measurand without a Bayesian adjustment (i.e., the mean of the n observations of the current measurement).

The scatter plots of the simulated expanded uncertainty help visualize the random error and bias associated with the uncertainty calculation models. In the following sections, we present theoretical analysis and Monte Carlo simulation results that quantitatively characterize the random error and bias.

Random Error of Uncertainty Calculation Models

The random error of an expanded uncertainty estimate is measured by the relative standard deviation (*RSD*), which is the ratio of the population standard deviation of U_s to the true uncertainty U

$$RSD = \frac{\sigma[U_s]}{U} \quad . \qquad (10)$$

Thus, the RSD for the Student's t model is

$$RSD = \frac{t_{95}}{z_{95}} \frac{\sigma[s[\bar{q}]]}{\sigma[\bar{q}]} \tag{11}$$

and the RSD for the Craig model is

$$RSD = \frac{1}{c_4} \frac{\sigma[s[\bar{q}]]}{\sigma[\bar{q}]}, \tag{12}$$

where $\frac{\sigma[s[\bar{q}]]}{\sigma[\bar{q}]} = \frac{\sigma[s[q]]}{\sigma[q]} = \frac{\sqrt{1-c_4^2}}{c_4} \approx \frac{1}{\sqrt{2(n-1)}}$, which can be found in a statistics textbook, for example, Wadsworth (1989).

The analytical expression for the *RSD* for the Bayesian model is not available. Figure 2 shows a comparison of the *RSD* for the three models. The *RSD* for the Bayesian model is generated from the Monte Carlo simulation with the assumption that the prior standard deviation is equal to the population standard deviation. The simulated *RSD* is independent from the population mean and standard deviation used in the simulation.

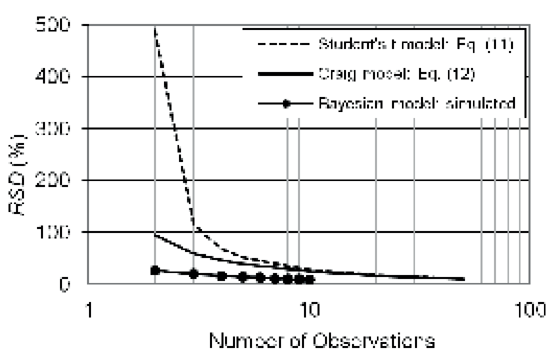

Figure 2. Comparison of RSD.

It can be seen from Figure 2 that, among the three models, the Student's *t* model has the highest *RSD*, the Bayesian model has the lowest, and the Craig model is in the middle. The *RSD*s are 490%, 115%, and 69% for the Student's *t* model, 26%, 20%, and 16% for the Bayesian model, and 95%, 59%, and 46% for the Craig model, at n=2, 3, and 4, respectively. The reason for the Bayesian model's low *RSD* is the use of prior information.

Bias of Uncertainty Calculation Models

The bias of an expanded uncertainty estimate is measured by the relative bias (*RB*), which is the difference between the mean of *U*s and the true uncertainty *U*, relative to the true uncertainty *U*

$$RB = \frac{\overline{U_s}}{U} - 1 \tag{13}$$

where $\overline{U}_s$ is the mean of U_s.

The relative bias of the Student's *t* model is

$$RB = \frac{c_4 \; t_{95}}{z_{95}} - 1\,. \tag{14}$$

The relative bias of the Craig model is zero (Huang 2010). The analytical expression for the *RB* of the Bayesian model is not available. Figure 3 shows a comparison of the relative bias of the three models. The *RB* for the Bayesian model is generated from the Monte Carlo simulation with the assumption that the prior standard deviation is equal to the population standard deviation. The simulated *RB* is independent from the population mean and standard deviation used in the simulation.

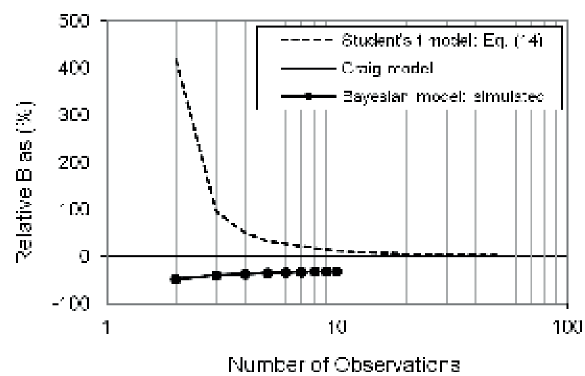

Figure 3. Comparison of relative bias.

It can be seen from Figure 3 that the *RB* of the Student's *t* model is very high for small samples. For example, the *RB*s are 417%, 95%, and 50% at n=2, 3, and 4, respectively. It is still 12% at n=10. This means that Student's *t* model is inaccurate for small samples. On the other hand, the Craig model has zero bias for any number of observations, so it is accurate for estimating the true uncertainty of the measurand (without the Bayesian adjustment). Note that the Bayesian model has a negative bias from the true uncertainty. This is expected because the true standard uncertainty is used as the prior standard uncertainty in the Monte Carlo simulation, i.e., $s_P[\bar{q}] = \sigma[\bar{q}]$ in Eq. (6). Thus, no matter what the ratio γ is, the uncertainty calculated using the Bayesian model will be smaller than the true uncertainty.

Discussion on the Extreme Case: *n*=2

Two observations (*n*=2) is the extreme case for repeated measurements. In practice, obtaining more than two observations may be impractical due to high cost, a time-consuming process in conducting the measurement, or a change in measurement conditions. An example of such situations we discuss here is the river discharge measurement. The current-meter method for a river discharge measurement may take about one hour in a medium-sized river. The standard practice is to make only one measurement and estimate the uncertainty of the single measurement using a Type-B evaluation. The revolutionary ADCP (acoustic Doppler current profile) method takes much less time in comparison to the current-meter method, but it is still costly and time consuming for large rivers. In addition, a change in river flow may not allow multiple discharge measurements to be conducted within a short time span, say, a half hour, in a tidal river. The current ADCP river-discharge-measurement quality control policy requires four measurements for a steady-flow river (e.g., Oberg et al 2005). Apparently, it will be a significant cost and time saver if the requirement can be reduced to two measurements.

Suppose that only two observations (two transect discharge measurements of ADCP) are made and we want to know the expanded uncertainty associated with the mean of the two observations. The question, then, is which model is appropriate and should be used? Here, we assume no prior information is available. Therefore, only the Student's *t* model and the Craig model are considered.

The previous analysis indicates that the *RSD* and *RB* at *n*=2 are 490% and 417%, respectively, for the Student's *t* model. This means that the Student's *t* model is extremely imprecise and inaccurate for estimating the uncertainty associated with two observations. On the other hand, the *RSD* and *RB* at *n*=2 are 95% and 0%, respectively, for the Craig model. Therefore, the Craig model should be more appropriate than the Student's *t* model.

Table 1 shows three data sets for discharge measured by ADCPs at three sites. The first data set was collected in the Mississippi River on January 30, 1992 (Gordon 1992). A total of 30 transect discharges were collected at this site during a steady-flow condition. Only the first four are used here. The second data set was collected at the Yangtze River on September 20, 2002 and the third at an irrigation canal in the Imperial Irrigation District in California on December 10, 2003. The author was involved in the field work for collecting these two data sets.

The quality of the river discharge measurement may

	Discharge (m^3/s)			
	Transect 1	Transect 2	Transect 3	Transect 4
Mississippi River*	14101	14470	14438	14500
Yangtze River	11234	11582	11485	11476
Irrigation Canal	4.08	4.2	4.14	4.22

* A total of 30 transect discharges were collected at this site (Gordon 1992). Only the first four are shown and used.

Table 1. Discharge measured by ADCP at three sites.

	Mean (m^3/s)	Standard deviation (m^3/s)	*REU* (%)	
			Student's *t* model	Craig model
Mississippi River	14377	185.9	2.06	1.38
Yangtze River	11444	148.2	2.06	1.38
Irrigation Canal	4.16	0.063	2.42	1.62

Table 2. Statistics and uncertainty-analysis results at n=4.

	Mean (m^3/s)	Standard deviation (m^3/s)	*REU* (%)	
			Student's *t* model	Craig model
Mississippi River	14286	260.9	16.41	3.17
Yangtze River	11408	246.1	19.38	3.75
Irrigation Canal	4.14	0.085	18.41	3.56

Table 3. Statistics and uncertainty-analysis results at *n*=2 (the first two transects).

be evaluated in terms of the uncertainty associated with the mean of transect discharges. The maximum permissible relative uncertainty, *MPRU*, for river discharge measurement quality control is as follows (Huang 2008)

$$REU \leq MPRU = \begin{Bmatrix} 6.1\% & at\ n=2 \\ 4.3\% & at\ n=4 \end{Bmatrix}. \quad (15)$$

Tables 2 and 3 show the statistics and uncertainty-analysis results using the Student's *t* and Craig models for the four and two transects (the first two transects), i.e., *n*=4 and 2, respectively.

It can be seen from Table 2 that the *REU* calculated using either the Student's *t* or Craig model is less than the *MPRU* of 4.3% at *n*=4. This means the measurements at these three sites are satisfactory. However, it can be seen from Table 3 that the *REU* calculated using the Student's *t* model is much greater than the *MPRU* of 6.1% at *n*=2. The approximate true uncertainty for the Mississippi River discharge (estimated from all of the 30 transect discharges) is only 2.17% at *n*=2. Therefore, the *REU* at n=2 calculated using the Student's *t* model is paradoxical and misleading due to both the high random error and bias of the model. On the other hand, the *REU* at *n*=2, calculated using the Craig model, is less than the *MPRU* of 6.1% at *n*=2, which is consistent with the *n*=4 results.

Therefore, for the ADCP river discharge measurement, two observations may be acceptable if the evaluation of the expanded uncertainty is obtained by using the Craig model. The Student's *t* model should not be used in this case. The same conclusion may apply to other fields of measurements.

Conclusion

The expanded uncertainty calculated using the experimental standard deviation may contain random error and bias. The Student's *t* model has much a higher random error than either the Craig or Bayesian model. It also has a significant bias from the true uncertainty for small samples. The Craig model has zero bias for any number of observations. That is, the Craig model offers an unbiased estimate of the true uncertainty.

Because of the high random error and bias, the uncertainty calculated using the Student's *t* model is paradoxical and misleading for small samples. Therefore, the Student's *t* model should not be used for small samples, say, *n*=2, or 3. On the other hand, the uncertainty calculated using the Craig or Bayesian model is reasonably accurate even at *n*=2 or 3.

In summary, among the three models, the Student's *t* model is the least precise and accurate, the Craig model is more precise and accurate than the Student's *t* model, and the Bayesian model is the most precise and accurate because of its use of prior information. When prior information is available, the Bayesian model is preferred for calculating the expanded uncertainty. When prior information is not available, the Craig model is preferred.

References

Airy GB. 1861. *On the algebraical and numerical theory of error of observations and the combination of observations* Cambridge and London: Macmillan and Co.

Craig CC. 1927. Remarks on the probable error of a mean *The American Mathematical Monthly* **34**(9) 472-76.

Gordon RL. 1992. *Mississippi River Discharge* RD Instruments Report.

Huang H. 2010. A paradox in measurement uncertainty analysis, Presented at the 2010 Measurement Science Conference in Pasadena, CA, March 25 – 26, 2010. In *"Global Measurement: Economy & Technology," 1970 - 2010 Proceedings (DVD).*

Huang H. 2008. Estimating precision of moving boat ADCP discharge measurement *Proceedings (DVD) of 14th Australian Hydrographers Association Conference: Water Initiatives 2008 and Beyond* Canberra, Australia, August 2008.

ISO-GUM 1993 *Guide to the Expression of Uncertainty in Measurement* (corrected and reprinted in 1995) International Organization for Standardization, Geneva, Switzerland.

Oberg KA, Morlock SE and Caldwell WS. 2005. *Quality-Assurance Plan for Discharge Measurements Using Acoustic Doppler Current Profilers* U.S. Geological Survey, Scientific Investigations Report 2005-5183.

Phillips SD, Estler WT, Levenson MS and Eberhardt KR. 1998. Calculation of measurement uncertainty using prior information *J. of Research of the National Institute of Standard and Technology* **103**(6) 625-32.

Student. 1908. The probable error of a mean *Biometrika* **VI** 1-25.

Wadsworth Jr. HM. 1989. Summarization and interpretation of data in *Handbook of Statistical Methods for Engineers and Scientists*, ed. Harrison M Wadsworth Jr. McGRAW-HILL Inc. 2.1-2.21.

Hening Huang, Teledyne RD Instruments, 14020 Stowe Drive, Poway, CA 92064, USA, hhuang@teledyne.com.

This paper was previously presented at the 2011 Measurement Science Conference (MSC) in Pasadena, California, March 17-18, 2011.

Calibrating Low-Temperature Radiation Thermometers

Peter Saunders
Measurement Standards Laboratory of New Zealand

The advent of low-cost handheld radiation thermometers, or infrared (IR) thermometers, has led to a proliferation of non-contact temperature measurement in the food, building, and low-temperature processing industries. These thermometers typically measure temperatures in the range –50° C to 500° C using uncooled thermopiles that detect radiation in the 8–14 μm spectral range (or similar). However, these instruments are not as simple to use or to calibrate as they first appear due to systematic effects that are present in almost all measurements. This article provides information relating to the calibration of these "low-temperature" IR thermometers. Because the detectors in these instruments are uncooled, radiation emitted by the detector itself must be considered in the calibration process. The emissivity setting on the thermometer, which is often fixed at a value of 0.95, and any radiation reflected from the surroundings, must also be taken into account. As a consequence of these systematic effects, calibration methods are more complicated than for contact thermometers or high-temperature IR thermometers. The expected reading, even on a perfect IR thermometer, does not necessarily match the reading of the reference thermometer. This article describes the nature of the systematic effects and outlines a procedure for determining the corrections required during calibration.

Thermometer Response Function

In order to quantify and correct for the systematic effects during calibration of an IR thermometer, such as that shown in Figure 1, it is necessary to understand the relationship between the signal measured by the detector and the temperature reading on the thermometer's display. The basic relationship between signal and temperature for a blackbody source is given by a thermometer response function, which is well-approximated by the following equation, based on Planck's law (see Figure 2):

$$S(T) = \frac{C}{\exp\left(\frac{c_2}{AT+B}\right)-1} . \tag{1}$$

In equation (1), A, B and C are constants related to the properties of the IR thermometer, and c_2 is a universal constant with the value 14388 μm.K. For thermopile detectors, this signal takes the form of a voltage. Note that the value of T in equation (1) has the units of kelvin.

The thermometer response function represented by equation (1) is determined by the manufacturer during the initial set-up calibration, and the measured signals are processed internally to give a temperature reading on the device, with the details of this process not normally available to the user. The manufacturer may not use equation (1) explicitly as the response function, but whatever is implemented, such as a look-up table, will be equivalent to equation (1).

During subsequent re-calibration of an IR thermometer, a calibration laboratory needs to apply corrections to the detector signals based solely on the temperature indications, so knowledge of the details of the thermometer response function is required since the detector signals are not available directly. Ultimately, conversion from signal to temperature must also be carried out, and this can be accomplished using the inverse of equation (1):

$$T = \frac{c_2}{A\ln(C/S+1)} - \frac{B}{A} . \tag{2}$$

Evaluation of equations (1) and (2) requires knowledge only of the thermometer parameters A and B. It turns out that the value of C is unimportant, as long as the same

Figure 1. A typical low-temperature handheld infrared thermometer. Photo courtesy of Fluke Corporation, reproduced with permission.

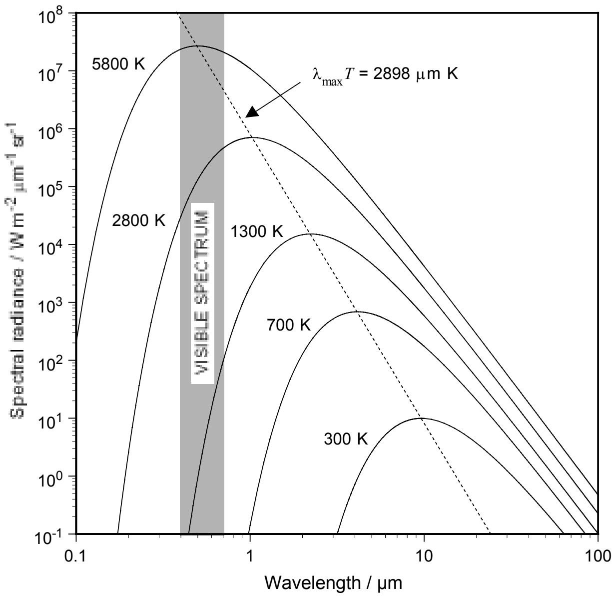

Figure 2. Spectral radiance of a blackbody at various temperatures, as given by Planck's law. The signal response of an IR thermometer, equation (1), is proportional to the area under these curves between the wavelength limits of the thermometer's spectral response (e.g. between 8 μm and 14 μm). The peak of the spectral radiance curves shifts to shorter wavelengths with increasing temperature (dotted line). Our eyes have evolved to be most sensitive at wavelengths corresponding to the peak of sun's spectrum (at 5800 K), as indicated by the shaded band of the visible spectrum.

value is always used for all calculations. Therefore, we can simply assign $C = 1$ in the evaluation of equations (1) and (2). A and B are both related to the wavelength range over which the IR thermometer operates:

$$A = \lambda_0\left(1 - \frac{\Delta\lambda^2}{2\lambda_0^2}\right) \quad (3)$$

$$B = \frac{c_2\Delta\lambda^2}{24\lambda_0^2}, \quad (4)$$

where λ_0 is the centre wavelength of the range and $\Delta\lambda$ is the width of the wavelength range. Thus, for an IR thermometer operating from 8–14 μm, we get $\lambda_0 = 11$ μm and $\Delta\lambda = 6$ μm, and equations (3) and (4) give $A = 9.36$ μm and $B = 178$ μm.K, respectively.

While many low-temperature IR thermometers operate over this wavelength range of 8–14 μm, there are many other ranges also in use, such as 8–13 μm and 7–18 μm. It is important to check the specifications to determine the actual wavelength range used.

Thermometer Measurement Equation

The signal at the output of the detector of an IR thermometer corresponds to the difference between the radiation incident on the detector and the radiation emitted by the detector itself due to its finite temperature. The incident radiation generally consists of two components: the radiation emitted from the target, and the radiation reflected off the target that originates from the target's surroundings (see Figure 3).

Thus, the measured signal, S_{meas}, can be written as the sum of three components:

$$S_{meas} = \varepsilon_s S(T_s) + (1-\varepsilon_s)S(T_w) - S(T_d), \quad (5)$$

where T_s is the temperature of the target (the quantity of interest), T_w is the temperature of the surroundings (often the walls of the room), T_d is the temperature of the detector, ε_s is the emissivity of the target's surface, and $1 - \varepsilon_s$ is its reflectivity. Each of the *S(T)* quantities can be calculated using equation (1) by inserting the appropriate *T* value.

If the measured signal, S_{meas}, given by equation (5) is substituted into the signal-to-temperature conversion equation (2), the result will not be the target temperature T_s, because of the influences of the target emissivity, the temperature of the surroundings, and the temperature of the detector (ε_s, T_w, and T_d). In order to produce a reading that better represents the target temperature, the IR thermometer pre-processes the measured signal before conversion to temperature, in effect applying corrections for the above influences. To do this reliably, the thermometer must somehow obtain values for the three influence variables, ε_s, T_w, and T_d.

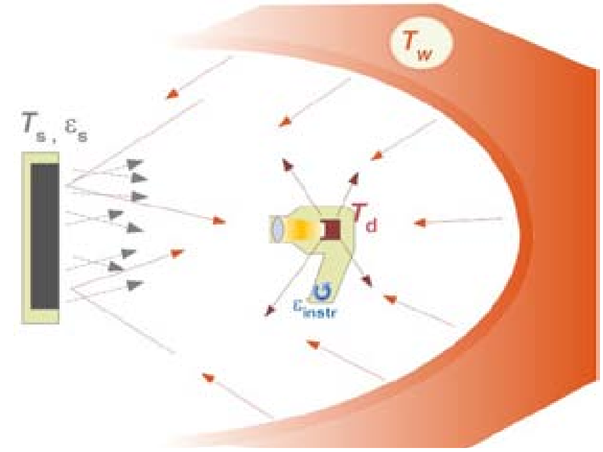

Figure 3. The detector signal is equal to the difference between the incident radiation from the target (emitted and reflected) and the radiation emitted by the detector itself. Drawing courtesy of Kelvin-Trainingen, reproduced with permission.

The detector temperature, T_d, is accurately determined by using an internal temperature probe mounted directly on the detector. Its measurement occurs automatically as part of the IR thermometer's measurement process and is completely hidden from the user.

For IR thermometers with an adjustable instrumental emissivity setting, ε_{instr}, the user can inform the thermometer of the value of the target emissivity by setting ε_{instr} accordingly. Some instruments, however, have a fixed emissivity setting, usually 0.95 or 0.97. These instruments are designed for specific applications, such as in the food industry where many of the plastic and cardboard packaging materials have emissivities close to 0.95 in the 8–14 µm range. In fact, most organic materials, such as wood, paint, and skin, and even water and ice, also have emissivities near 0.95 in this infrared region, so there are a wide range of applications suitable for these fixed-emissivity instruments.

Finally, the temperature of the surroundings, T_w, will depend on the measurement situation, and will vary from measurement to measurement. For this influence variable, most IR thermometer manufacturers make the implicit assumption that T_w will be approximately the same as the detector temperature, T_d. In other words, they assume that all measurements are to be performed in ambient surroundings. This assumption is usually fine during calibration in a well-controlled laboratory, but it can be quite misleading in other measurement situations. These include cool stores, where the temperature of the surroundings is well below the temperature of the thermometer, and situations where products to be measured are surrounded by hot objects, such as heaters, which are well above the temperature of the thermometer.

Armed with this information, the IR thermometer processes the measured signal as follows: first the measured signal is divided by the instrumental emissivity setting; then a quantity corresponding to the signal at the detector temperature is added; finally, the resulting signal value is converted to a measured temperature value, T_{meas}. This is represented mathematically as:

$$S(T_{meas}) = \frac{S_{meas}}{\varepsilon_{instr}} + S(T_d)\ . \qquad (6)$$

Measurement Errors

To understand the consequences of this signal processing, we can substitute S_{meas} from equation (5) into equation (6):

$$S(T_{meas}) = \frac{\varepsilon_s S(T_s) + (1-\varepsilon_s)S(T_w) - (1-\varepsilon_{instr})S(T_d)}{\varepsilon_{instr}}\ . \qquad (7)$$

The difference between T_{meas} and T_s is the error in the thermometer's reading. To clarify the error, equation (7) can be rewritten as the sum of three terms:

$$\begin{aligned} S(T_{meas}) &= S(T_s) \\ &+ \frac{(1-\varepsilon_{instr})}{\varepsilon_{instr}}\left[S(T_w) - S(T_d)\right] \\ &+ \frac{(\varepsilon_s - \varepsilon_{instr})}{\varepsilon_{instr}}\left[S(T_s) - S(T_w)\right]. \end{aligned} \qquad (8)$$

If the second and third lines of this equation are both zero, then the equation is simply $S(T_{meas}) = S(T_s)$, implying that $T_{meas} = T_s$. However, when either of the second or third lines of the equation is not zero, they represent error terms. In this case, the measured temperature is no longer equal to the target temperature.

The second line is zero when either $\varepsilon_{instr} = 1$ or $T_w = T_d$. The condition $T_w = T_d$ is the manufacturers' assumption mentioned above. Equation (8) allows the error to be quantified when this condition doesn't hold. Setting $\varepsilon_{instr} = 1$ (if possible) is often a good strategy because then the measured temperature, T_{meas}, is independent of T_d. However, this may introduce error through the third line in equation (8).

This third line is zero when either $\varepsilon_{instr} = \varepsilon_s$ or $T_s = T_w$, that is, when the instrumental emissivity matches the emissivity of the target, or the target temperature is the same as the temperature of the surroundings. Incorrectly setting the instrumental emissivity leads to an error that increases as the difference between these two temperatures increases. The user has no control over this error for fixed-emissivity instruments, unless the condition $T_s = T_w$ holds.

Calibration

The errors discussed above occur in almost all measurements with IR thermometers, and care must be taken to ensure that these errors are not excessive. They also occur during calibration because the conditions for which the errors are zero ($T_w = T_d$ and $\varepsilon_{instr} = \varepsilon_s$) very rarely both hold. This raises the issue of how to calibrate an IR thermometer when errors are expected in the readings, even for a perfect thermometer. The solution is to first calculate the expected readings for an ideal device under the calibration conditions and compare how close the actual readings are to the expected ones, or, equivalently, to calculate "blackbody corrections," which are applied to the reference thermometer readings before comparing with the readings of the device under calibration.

Conventional blackbodies used for calibration are made from cavities so that their effective emissivity is very close to 1.

These blackbody cavities include purpose-built furnaces (see Figure 4) and inserts into dry-block calibrators. The effective emissivity of a cavity, ε_{bb}, can be estimated from its length L, the radius of its aperture, r, and the emissivity of the material from which it is made, ε_s (see Figure 5):

$$\varepsilon_{bb} = 1 - (1 - \varepsilon_s)\left(\frac{r}{L}\right)^2 . \quad (9)$$

For example, a cavity made out of a material that has an emissivity of 0.9 (oxidised stainless steel), whose length is 150 mm and whose aperture radius is 25 mm, has an effective emissivity of $\varepsilon_{bb} = 0.997$.

Figure 4. A blackbody cavity, with a length of 200 mm and maximum aperture diameter of 120 mm, enclosed in a uniform-temperature furnace. The effective emissivity is at least $\varepsilon_{bb} = 0.991$.

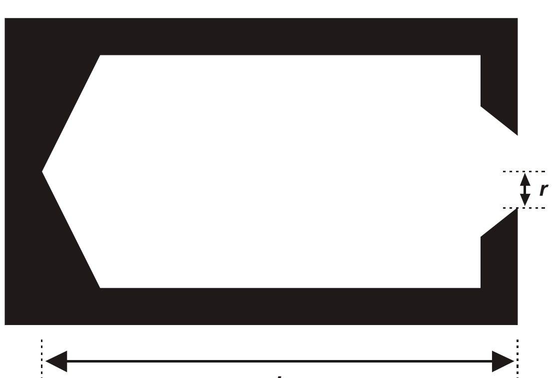

Figure 5. A blackbody cavity of length L and aperture radius r, whose walls have an emissivity ε_s. The effective emissivity of the cavity is given by equation (9). In use, the cavity is heated uniformly in a furnace or dry-block calibrator.

Figure 6. A flat-plate calibrator, with a diameter of 150 mm and emissivity of 0.95, being viewed by an infrared thermometer. Photo courtesy of Fluke Corporation, Hart Scientific Division, reproduced with permission.

Figure 7. Measurement of an ice-point blackbody. The blackbody is a cavity carved into shaved melting ice inside a Dewar. While the ice is melting, its temperature is naturally maintained at a temperature of 0° C, so a separate reference thermometer is not required (see Ref. [1] for more details concerning the ice point).

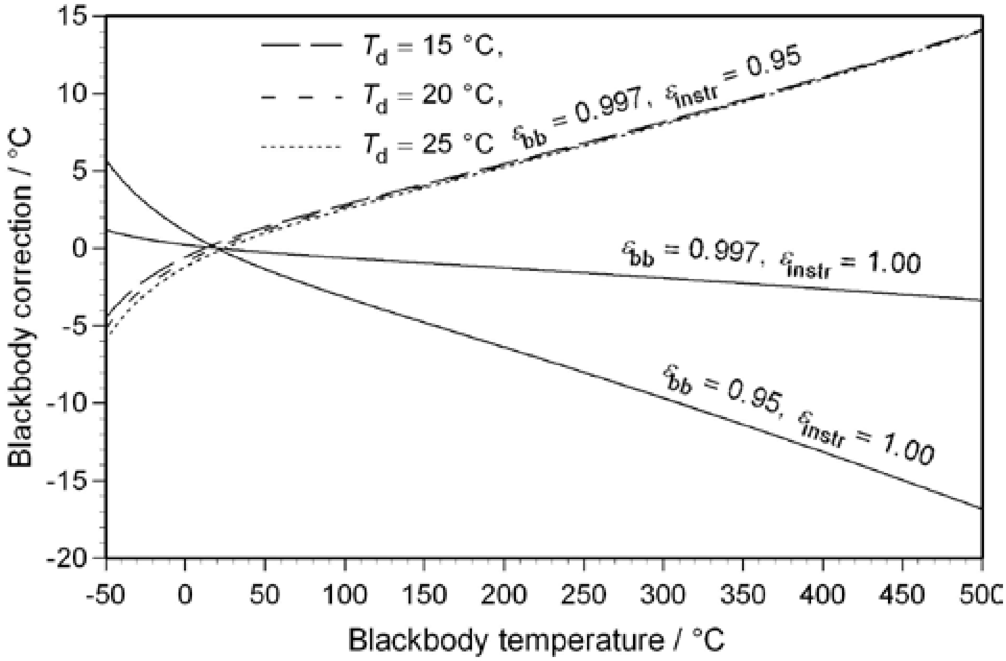

Figure 8. Blackbody corrections for various parameters for the calibration of an 8–14 μm IR thermometer. The ambient temperature is assumed to be T_{amb} = 20° C in all cases. The detector temperature is only important when $\varepsilon_{instr} < 1$.

Plate-flat calibrators are also used as blackbody sources (see Figure 6). However, their emissivity is usually close to 0.95, so they are not true blackbodies. For the purpose of this article, though, both types of calibration source will be referred to as blackbodies, and they will be distinguished by their effective emissivities.

The reference thermometer, which measures the true temperature of the blackbody, can be either a contact thermometer, such as a platinum resistance thermometer, or a reference infrared thermometer. In the special case of the ice-point blackbody at 0° C, no separate reference thermometer is required (see Figure 7).

In a calibration laboratory, the temperature of the surroundings is usually equal to ambient temperature, T_{amb}. Thus, equation (7) can be rewritten to give the expected thermometer reading, T_{exp}:

$$S(T_{exp}) = \frac{\varepsilon_{bb}S(T_{ref}) + (1-\varepsilon_{bb})S(T_{amb}) - (1-\varepsilon_{instr})S(T_d)}{\varepsilon_{instr}}, \quad (10)$$

where ε_{bb} is the effective emissivity of the blackbody and T_{ref} is the true temperature of the blackbody, as determined by the reference thermometer. The second term in the numerator of equation (10) corresponds to ambient radiation that enters the blackbody cavity from the surroundings and finds its way back out, or the radiation that is reflected off the flat plate. For the case of the cavity, whose effective emissivity is generally very close to 1, this term will be very small.

For a given set of conditions, the expected temperature can be calculated by evaluating the right-hand side of equation (10) (with the aid of equation (1) to determine $S(T_{ref})$, $S(T_{amb})$, and $S(T_d)$), thus giving $S(T_{exp})$, then equation (2) can be used to extract T_{exp} from $S(T_{exp})$. The blackbody correction, ΔT_{bb}, is the difference between the expected reading and the true temperature of the blackbody, as determined by the reference thermometer:

$$\Delta T_{bb} = T_{exp} - T_{ref}\ . \quad (11)$$

This blackbody correction, in some cases, can be quite significant. These calculations are easily performed using a spreadsheet application.

T_{ref} (°C)	$S(T_{ref})$ [eq (1)]	$S(T_{amb})$ [eq (1)]	$S(T_d)$ [eq (1)]	$S(T_{exp})$ [eq (10)]	T_{exp} (°C) [eq (2)]	ΔT_{bb} (°C) [eq (11)]
–50	0.00175	0.00732	0.00744	0.00147	–56.5	–6.5
100	0.02025	0.00732	0.00744	0.02088	103.0	3.0
500	0.16773	0.00732	0.00744	0.17566	516.4	16.4

Table 1. Calculation of the blackbody corrections for three values of T_{ref} for an 8–14 μm IR thermometer (A = 9.36 μm, B = 178 μm.K) with ε_{instr} = 0.95, ε_{bb} = 0.997, T_{amb} = 20° C, and T_d = 21° C.

An example calculation is given in Table 1 for the calibration of an 8–14 μm IR thermometer whose instrumental emissivity is fixed at 0.95, using a blackbody cavity with an effective emissivity of 0.997. In the example, the ambient temperature is 20° C and the detector temperature is 21° C. Note the detector temperature is not generally known, as it is not usually displayed on the device, so its value must be approximated, or guessed at, in order to calculate the blackbody corrections when ε_{instr} is not set to 1.

Figure 8 shows the blackbody corrections for the entire range of blackbody temperatures from –50° C to 500° C for various combinations of ε_{bb} and ε_{instr} (the curves with $\varepsilon_{bb} = 0.997$ correspond to a cavity, and those with $\varepsilon_{bb} = 0.95$ to a flat-plate calibrator). The corrections are smallest when $\varepsilon_{instr} \approx \varepsilon_{bb}$. Also shown is the effect of various detector temperatures in the case when $\varepsilon_{instr} < 1$. The detector temperature may differ from ambient temperature if the thermometer has been stored in a room at a different temperature to that of the calibration laboratory and not given time to equilibrate before measurements are made. The detector may also become warmer than ambient if placed in front of a hot blackbody for a length of time. As Figure 8 shows, there is only a weak dependence of the blackbody correction on detector temperature, mainly at lower temperatures. The bulk of the correction is due to the fact that $\varepsilon_{instr} \neq \varepsilon_{bb}$.

The calibration procedure is summarized by the following steps:

1. Determine the minimum and maximum wavelengths for the operating wavelength range of the device under calibration. These should be stated in the thermometer's specifications under "spectral response."
2. Using these values in equations (3) and (4), calculate the A and B coefficients of the thermometer response function.
3. Determine the blackbody emissivity, ε_{bb}, either as an effective value from equation (9) for a cavity, or directly from the specifications for a flat-plate calibrator.
4. Set the instrumental emissivity, ε_{instr}, as close as possible to ε_{bb} (unless requested otherwise by the client), or if the instrumental emissivity is fixed, determine its value from the thermometer's specifications.
5. Measure the ambient temperature, T_{amb}, with an air-temperature probe or with an IR thermometer aimed at the wall.
6. Estimate the detector temperature, T_d. This is likely to be the same as ambient temperature provided the IR thermometer has had sufficient time to equilibrate with the calibration laboratory and if the IR thermometer is not heated excessively by radiation from the blackbody. If the instrumental emissivity is set to 1, the value of T_d is not required.
7. For each calibration point, determine the true temperature of the blackbody, T_{ref}, using the reference thermometer and calculate the expected IR thermometer reading, T_{exp}, using equation (10). Compare the actual reading on the IR thermometer with the value of T_{exp}. The difference between the expected temperature and the actual reading is the correction that should be reported on the calibration certificate for that calibration temperature.

Conclusion

This article has given a brief overview of some of the considerations necessary when calibrating low-temperature IR thermometers. Emphasis has been placed on the signal processing algorithm implemented by these thermometers, which means that the expected thermometer reading may differ from the true temperature of the blackbody calibration source. A major consideration not discussed here is the size-of-source effect, which can lead to significant errors in use if the target size differs from that used during calibration.

Further details on the calibration process, including simplifications when using an IR thermometer or the ice point as the reference, can be found in [2], and procedures for determining and correcting for the size-of-source effect can be found in [3].

References

[1] MSL Technical Guide 2: "Infrared Thermometry Ice Point," http://msl.irl.cri.nz.
[2] MSL Technical Guide 22: "Calibration of Low-Temperature Infrared Thermometers," http://msl.irl.cri.nz.
[3] MSL Technical Guide 26: "Size-of-Source Effect for Direct-Reading Radiation Thermometers," http://msl.irl.cri.nz.

Peter Saunders, Measurement Standards Laboratory of New Zealand, p.saunders@irl.cri.nz.

CLASSIFIEDS

Alaska Metrology & Calibration Services

Sita Schwartz
Cal Lab Editor

This editor recently networked up with business owner, Clinton Schirard, out of Anchorage, Alaska. His situation is unique in that he operates a mobile unit in an especially extreme environment. How many cal labs can say the melting of an ice-road dictates their schedule? Last year, we featured an article that proposed a mobile flow testing unit in another extreme environment, the arid desert, but in theory only. Here, we get the details of a working mobile calibration unit operating in another extreme, arid environment—on the North Slope of Alaska.

Living in Alaska

The environment on the North Slope is unique to say the least. At a latitude of 70°19'00N, daylight can be anywhere from 2 hours long during November to 24 hours long from mid-May through July. Temperatures can be as high as 60° F in the summer and -50° F in the winter. Wind chills can get down to -100° F during a blizzard. Precipitation is minimal, with an average of 5 inches a year.

The physical environment, the native people and animals, and the oil industry set Alaska apart from any other experience. The brutally cold environment is so extreme, "it is like being on another planet" says Clinton Schirard, owner of Alaska Metrology & Calibration Services (AMCS). The cold and miserable climate of somewhere within the contiguous states is totally unlike the cold of the North Slope. For Clinton, this extreme is what makes Alaska so unique. "Summer is a marked relief" when it comes and "everything is so green and alive, it's like a night and day difference." This unique environment reflects upon the native villages that exist on the North Slope. Vehicles are able to drive right up along the frozen rivers to gain access to remote villages. Each village is exclusive to itself: some are well-kept and the people friendly and warm, while another village might be run down and the people not so nice. Each village might also have a specific place, such as a landmark or church, which sets it apart from another village.

The oil industry creates land locked operational sites named after drilling activities. Access is limited to air travel and private roads. Human activity revolves around the oil industry, whether they are tourists traveling through, or providers of a service supporting the industry. Even the native people are not isolated from the industry, as they are affected one way or another.

Side view of the 45' mobile calibration lab.

The Mobile Calibration Unit

AMCS operates out of Anchorage, Alaska, with eight mobile laboratory sites located on the north end of the state, in and around Prudhoe Bay, on the edge of the Arctic Ocean. They calibrate and repair commercial test and measurement instruments for clients working in Alaska's oil & gas, aviation, public transportation, military, construction and safety industries.

AMCS owns and operates a mobile calibration lab that travels to production sites—adjacent to electrical warehouses, machine shops, etc.—in some of the most challenging environments on the planet. Some of the largest oil fields in North America can be found here on the North Slope of Alaska. Mobile units, such as those owned and operated by AMCS, provide critical services to the petroleum, construction, and aviation industries in remote areas.

The mobile calibration unit is located at each site for about one to two months at a time, contracted out to British Petroleum and ConocoPhilips, as well as other companies operating in Prudhoe Bay, Kuparuk, Oiliktok Point and Alpine. The mobile unit travels to centralized facilities that maintain and control the wells that feed into the Trans Alaska Pipeline, which runs from Prudhoe Bay, in the north, down to Valdez, in the south. AMCS's mobile calibration lab is their newest unit: a 45 foot long enclosed container trailer, equipped with standards for maintaining precision and construction tools for about 25 different clients in the oil industry. This latest unit features an Arctic Entry, fire escape, 3-phase power transformer, built-in computer network cabling, and lots of lighting. The flooring is a rubberized non-skid surface while the interior walls and ceiling are finished with fiber-reinforced polymer.

Both units are powered by 3-phase 480 VAC power transformers to provide 120/208 power to the enclosed equipment and environmental controls. The newer mobile unit has a 2000 watt heating and air-conditioner unit mounted in a room accessible from the rear of the trailer. The trailer provides calibrations of tools such as electrical safety equipment and multimeters, pressure gauges, and torque wrenches. The calibration standards

AMCS's mobile calibration lab is their newest unit: a 45 foot long enclosed container trailer, equipped with standards for maintaining precision and construction tools for about 25 different clients in the oil industry.

include a Fluke 5520, Tektronics 3458A, Ruska 2485/2465A, and a CDT Sure-Test 2000. The readings are stored in a network of computers running Fluke's MET/Track® and MET/CAL®; certificates are issued from the mobile lab unit printers and distributed to shop foremen at client facilities.

The mobile unit is staffed by technicians in alternating two to three week shifts. They work 12 hours for the main contractors and additional hours as necessary for other companies needing calibration services. Technicians sleep and eat at large residential facilities that house other oil industry workers.

Logistical Challenges

Mobile calibration units, whether they serve a remote military base or a commercial operation, each have their own set of logistical challenges. For AMCS, location schedules are dictated by the ice. The end of one season and the beginning of another can trigger an evacuation to get out the area before the melting of the ice, or face getting stranded until next winter. Much of the land in and around Prudhoe Bay is leased or owned by oil companies who operate facilities visited by the mobile units. These facilities are often only accessible by ice-roads that form in the middle of winter.

For AMCS, the year begins in March at the Alpine station, at the edge of the National Petroleum Reserve. The mobile calibration unit stays through April 15th, when the road closes due to melting. From there, the unit travels to Milne Point and stays until June 1st. The next is stop is in Kuparuk, serving three facilities (CPF1, CPF2, and CPF3) until October. October is mostly spent at Deadhorse working for support services of the petroleum industry, before heading back to Prudhoe Bay. Work at Prudhoe Bay begins at the western side, the Base Operation Center (BOC), from November until January, before moving on to the east side of Prudhoe Bay, and then back again to the Alpine station in March.

As of the writing of this article, a bridge over the Colville River is being planned, which will provide year round access to the Alpine oil field. The photo of the loaded trailer (following page) was taken just 50 feet from the Colville River. Currently, access is limited due to the delicate tundra and temporary ice roads. Access by air is also limited to weather conditions: if a fog rolls in travelers can be grounded for days on end. So, improved access, such as a bridge to satellite oil fields, translates to more business for oil companies and their vendors.

The Growth of AMCS

The company was founded by Clinton Schirard who first came to Alaska in 1994 after graduating with a physics degree from Fort Lewis College in Durango, Colorado. He started off working at an electronics store, and then went to work for a small business which built electrical industrial control systems. After six years, he entered into calibration as a lab technician for a turbine engine manufacturer which had a side business providing on-site calibration services to two large oil companies in Prudhoe Bay, as well as several aircraft maintenance shops in Anchorage. Despite the good business on the calibration side, his employer was showing signs of shutting down business in Alaska.

In order to save their jobs, Clinton and several other employees took this opportunity to begin negotiating with another local business to buy-out the assets of the calibration shops owned by their employer, with the intent to start a standalone calibration business. Their plan fell apart when a key player got cold feet and walked away. But Clinton was now armed with all that he had learned through efforts to start a cal lab and was able to pull together a business plan, including all the other elements needed in order to strike out on his own.

In 2004, with a small business loan, he was able to buy out the calibration shop business from the turbine company. British Petroleum allowed the turbine company to sub-contract the remainder of the calibration contract. Clinton won two contracts the following year, allowing him to expand the business in Anchorage and Prudhoe Bay.

The next four years were good for AMCS, until the

A monochromatic light with two optical flats in the mobile calibration unit.

economy did a dive. In 2008, AMCS acquired a facility in Anchorage and received UL-508A listing to begin production of electrical control panels for new construction projects. The following year, their mobile unit, in use at the time in Prudhoe Bay, was destroyed due to a computer fire. This was a low point for the company; they were forced to stop work while they built a new mobile unit. But, after a rough 2009, the company has experienced steady growth.

Continuing Business Challenges

The next chapter for AMCS is acquiring ISO accreditation, in order to expand their customer base and remain competitive. A recent pre-audit went smoothly and provided the business with important steps it needs to take towards accreditation. One such step is being able to be one's own vendor—AMCS currently must send out their electronic torque bench to be calibrated. Once they are accredited, they will be able to calibrate their own electronic torque benches.

Another continuing challenge for doing business so far north is the availability of skilled labor. Hiring someone and bringing them out there is a big gamble for the small business owner. Once they arrive, are they what they say they are on paper? Without that face-to-face meeting, an employer doesn't have the advantage of a first-impression.

Ultimately, anyone who chooses the opportunity to live and work in a place with less creature comforts and outdoor recreation than, say, Durango, Colorado, must have an appreciation for such a place.

With society's increasing appetite for natural resources, Alaska's oil industry also requires solutions to its growing need for maintenance and production. AMCS found its niche in providing services to remote areas, along with production of goods: UL control panels and an injection monitoring system.

Acknowledments: Many thanks to Clinton Schirard for providing the material for this article. For more details on AMCS products and services, visit: http://www.akmetcal.com/.

This photo was taken April 2007 at a remote oil facility about 90 miles west of Prudhoe Bay known as Alpine, during an "evacuation" before the ice-road melts. Note the trucking company name on the side of the truck is one featured on the show "Ice Road Truckers" from the History Channel™.